Preprints of the 18th IFAC World Congress
Milano (Italy) August 28 - September 2, 2011

A Generic Approach to Missile Autopilot Design using State-Dependent Nonlinear Control

Tayfun Çimen*

** ROKETSAN Missiles Industries Inc., Ankara, TURKEY*
(e-mail: tcimen.control@gmail.com, tcimen@roketsan.com.tr).

Abstract: The fundamental objective of autopilot design for missile systems is to provide stability with satisfactory performance and robustness over the whole range of flight conditions throughout the entire flight envelope that missiles are required to operate in, during all probable engagements. Depending on the control mode (skid-to-turn or bank-to-turn), intercept scenario (such as surface to surface, surface to air, air to air) and mission phase (launch, midcourse, terminal), missile autopilots can command *accelerations*, *body rates*, *incidence angles*, or *flight path angles*. To this end, classical and modern multivariable techniques from linear control theory combined with gain scheduling have dominated missile autopilot design over the past several decades. In this paper, the concept of *extended linearization* (also known as *state-dependent coefficient parameterization*) is examined for *state-dependent nonlinear formulation* of the vehicle dynamics in a novel and very general form for the development of a generic and practical autopilot design approach for missile flight control systems. Any *extended linearization control method*, such as the currently popular State-Dependent Riccati Equation (SDRE) methods, can then be applied to this state-dependent formulation for missile flight control system design. The unique contribution of this paper is the novel use of a very general and realistic nonlinear aerodynamic model that captures all major aerodynamic nonlinearities attributed to missiles, together with the fully nonlinear and coupled 6-DOF equations of motion of rigid-body missile dynamics for full-envelope, 3-axes nonlinear autopilot design, without invoking any of the usual simplifying assumptions of the traditional linear design philosophy, and independent of any flight or trim conditions. Moreover, in the development of the generic approach, all the autopilot command structures mentioned above are incorporated in one compact topology. Practical considerations such as actuator dynamics and actuator position and rate saturation are also included in the development of the nonlinear autopilot. The proposed approach has been implemented and its performance and robustness validated in detailed 6-DOF simulations in three dimensional environments, using various missile configurations with stable, unstable and nonminimum-phase characteristics.

Keywords: Actuator saturation; Aerospace applications; Autopilot design; Flight control systems; Missile dynamics; Nonlinear control; Nonlinear systems; Optimal control; Riccati equations.

1. INTRODUCTION

Missiles are required to operate over a large flight envelope to meet the challenge of highly maneuverable targets in all probable engagements, such as surface-to-air and air-to-air missions against threats posed by both tactical aircraft and missiles. The fundamental objective of autopilot design for missile systems is to provide *stability* with satisfactory *performance* and *robustness* over the whole range of flight conditions that may be encountered throughout the flight envelope. However, the equations of motion that govern the behavior of a flight vehicle in six (three translational and three rotational) degrees of freedom (DOF) are both nonlinear and time varying, making flight control system design for missiles a complex, nontrivial multi-input–multi-output control problem. In view of the *uncertainties in aerodynamic parameters*, *cross-coupling effects*, *nonlinearities*, and *measurement inaccuracies*, the task of guaranteeing stability, performance and robustness throughout the entire flight envelope is a challenging one.

Conventional missile autopilot design is based on the application of linear control techniques to the decoupled and linearized longitudinal and lateral equations of motion of missile dynamics, neglecting all aerodynamic cross couplings between channels. Clearly, an autopilot derived from linearization about a single flight condition will be unable to achieve suitable performance over all envisioned operating conditions. Thus, standard practice in designing missile autopilots is to linearize the equations of motion for various flight conditions (around certain finite number of operating points and trim conditions in the flight envelope), and apply linear design techniques to these static models to deliver the desired performance characteristics in the local region of the fixed operating point. Satisfactory performance across the flight envelope may then be achieved by gain scheduling the resulting sets of local autopilot controller parameters as functions of the flight conditions (such as Mach number, altitude and angle of attack) to yield a global controller.

Although gain scheduling is the most prominent approach in missile autopilot design, there are some drawbacks to this design philosophy. The first is that due to wide variations in flight conditions, such as those encountered by high angle-of-attack missiles, linear autopilots require gain scheduling with respect to Mach number, altitude, angle of attack and sideslip angle. Therefore, depending on the mission and the flight

envelope, conventional autopilots with gain scheduling may necessitate controller design for several flight conditions. Although powerful classical and multivariable linear techniques are available for design, gain scheduling is a very tedious process that can consume an enormous amount of time and effort. Secondly, control design methods based on linear time-invariant models ignore the fundamental (nonlinear) nature of the plant for flight control systems. The controller so designed may offer unsatisfactory performance and are severely limited, especially when the dynamics is highly nonlinear and undergoes large motion. The ever increasing high performance and greater maneuverability requirements demand that missiles operate in regimes of large angles and angular rates, where nonlinearities are dominant and a high degree of coupling exists between the lateral and longitudinal motions because of inertial coupling. Under these circumstances, the assumption of small motion about an operating point does not hold true and nonlinear approaches must be employed for autopilot design.

In comparison to linear designs, nonlinear autopilots require significantly higher initial analysis effort, but are considerably easier to design than gain-scheduled linear controllers. Due to current technological trends and the sufficient computational resources that are nowadays available on-board, nonlinear autopilots have become viable candidates for implementation in missiles. Owing to these reasons and the severe nonlinear characteristics of flight vehicle dynamics at large angles and angular rates, there is obvious temptation for control designers to venture outside the linear design domain, and select nonlinear design methods.

In this paper, a generic and practical approach to nonlinear missile autopilot design is developed through a novel state-dependent nonlinear formulation of *missile aerodynamics* and *6-DOF rigid-body dynamics*, using the concept of *extended linearization*, also known as *state-dependent coefficient* (*SDC*) *parameterization* (Çimen, 2010). The development is pursued independent of any flight (or trim) condition and without invoking any of the usual simplifying assumptions in missile autopilot design, such as constant mass (post burnout), constant speed or constant air density, and without neglecting any cross coupling effects, such as roll rate, sideslip, and yaw rate. The design is based on a much more general and realistic missile model compared to the plethora of nonlinear approaches previously considered in the literature.

In the development of the nonlinear missile autopilot, all nonlinearities of missile dynamics are taken into full account. Specifically, the model captures all major nonlinear variations of the aerodynamic coefficients with flight parameters, and includes the inertial coupling between roll, pitch and yaw channels as well as the asymmetric structure of the missile airframe. The genericity to the approach is achieved through the use of a very general and realistic *nonlinear aerodynamic model* together with the fully coupled, *nonlinear model for the 6-DOF rigid-body dynamics*, by developing a high-performance, full-envelope, 3-axes nonlinear missile autopilot design concept. Through this genericity, the approach becomes applicable to both *skid-to-turn* (STT) and *bank-to-turn* (BTT) missiles (whether *canard*, *wing* or *tail* controlled), and during all phases of flight. More importantly, however, the design does not involve any decoupling of flight dynamics, does not require gain scheduling, is independent of trim conditions, and is very straightforward and practical.

The paper is organized as follows. For completeness, Section 2 first provides an overview of the general form of the 6-DOF rigid-body equations of motion for flight vehicle dynamics, clearly stating any assumptions, definitions and conventions used in deriving the model. These equations are required in deriving the nonlinear dynamic equations for state-dependent nonlinear formulation of the dynamics for missile autopilot design, and to illustrate how the 3-axes, coupled dynamics, which are valid at high angle of attack and sideslip angle, differ from conventional decoupled dynamics. The derivation of this nonlinear design model is presented in Section 3, along with actuator characteristics. For the purposes of this study, only aerodynamic control surfaces (canard, wing or tail) are considered as missile control effectors, leaving thrust vector control and reaction jet control thrusters as straightforward extensions of the developed approach. The proposed nonlinear autopilot topology, presented in Section 4, exploits the time-scale separation between the long-period (phugoid) and short-period modes, as well as between "slow" translational dynamics and "fast" rotational dynamics of the short-period mode inherent in missiles and other flight vehicles. In Section 5, the dynamics derived in Section 3 are formulated in state-dependent nonlinear form. In Section 6, a fully coupled, nonlinear approach is taken to design a high-performance, 3-axes, full-envelope missile autopilot based on the state-dependent nonlinear formulation of Section 5. In order to validate the satisfactory performance, robustness, genericity and practicality of the nonlinear missile autopilot design approach developed in this study, detailed 6-DOF nonlinear simulations have been carried out in three dimensional environments, under several noteworthy, realistic and coercive engagements, with various missile configurations. However, due to space limitations, only a brief discussion is pursued about the configurations tested, simulations performed and the results obtained, leaving discussions on design details, engagement scenarios, performance and robustness evaluations, and missile flight control system simulations for these test cases for presentation during the Congress. The paper is then closed with a brief summary in Section 7.

2. MISSILE FLIGHT DYNAMICS

2.1 Assumptions, Definitions and Conventions

The first objective is to derive the general form of equations of motion for a flight vehicle in 6 DOF (for further reading, readers may refer to Blakelock, 1991; Etkin, 2005; Stevens & Lewis, 2003; Zipfel, 2007). The derivation is carried out under the following assumptions:

A1) The effects of structural deflections (aeroelasticity) and of the dynamics of the relative motion of the control surfaces on overall missile dynamics are neglected, such that missile dynamics is based on the equations of motion for a single rigid body.

A2) The rotation of the Earth is neglected, with the curved surface (longitude/latitude grid) of the fixed Earth unwrapped into a flat plane tangential to the launch point. This is the so called stationary and flat-Earth

approach applicable to in-atmosphere, Earth-bound flights, valid for vehicles flying in the atmosphere with speeds less than Mach 5 (below hypersonic speed).

A3) The air is assumed to be at rest, neglecting any effect caused by wind.

A4) Gravity is assumed to be acting through the center of mass of the missile, so that missile center of mass (CM) coincides with missile center of gravity (CG).

Note that these are standard assumptions for deriving the 6-DOF rigid-body equations of motion of a flight vehicle, and all are applicable to tactical missiles and, with the exception of Assumption A3, to aircraft as well.

For modeling the motion of a rigid-body flight vehicle under Assumption A1, two *reference frames* are introduced. They are the *fixed-Earth frame* $\mathcal{F}_E(O_E; \mathbf{i}_E, \mathbf{j}_E, \mathbf{k}_E)$ and the missile *body-fixed frame* $\mathcal{F}_B(O_B; \mathbf{i}_B, \mathbf{j}_B, \mathbf{k}_B)$, whose triad of unit base vectors are orthonormal and right-handed by convention. The axes of the *coordinate systems* associated with each of the frames $\mathcal{F}_E$ and $\mathcal{F}_B$ are aligned with their respective triads, as shown in Fig 1. Due to assumption A2, the fixed-Earth frame $\mathcal{F}_E$ is declared as an inertial (Newtonian) reference frame. Its origin O_E is defined as the launch point of the missile, with X_E-axis pointing North, Y_E-axis pointing East, and the positive Z_E-axis pointing downward in the direction of the local gravity vector. The body-fixed frame $\mathcal{F}_B$ has its origin O_B located at the instantaneous CM of the missile, the X_B-axis is parallel with the body longitudinal centerline and points toward the nose of the missile, the Y_B-axis is directed to the right when viewed from the rear, and the Z_B-axis points in a direction below the horizontal. The three Euler angles ϕ, θ and ψ in roll, pitch and yaw, respectively, then describe the instantaneous angular orientation of the body coordinate system relative to the Earth coordinate system.

In the sequel, 6-DOF rigid-body nonlinear equations of motion will be derived, and then resolved in the body reference frame, such that all components of forces and moments acting on the missile will be modeled in the missile body-fixed axes. Fig. 1 shows the conventions used for positive directions of the vector components of force, moment, linear (translational) velocity, and angular (rotational) velocity of a missile resolved in the body coordinate system. The nomenclature adopted here is presented in Table 1. The six projections of the linear and angular velocity vectors on the moving body coordinate axes are the six degrees of freedom.

As the vehicle moves through the air mass, it experiences a relative wind over its body, which gives rise to aerodynamic forces. Introducing the *wind frame* $\mathcal{F}_W$, such that its X_W coordinate axis lies along the velocity vector $\mathbf{V}$ of the vehicle CM w.r.t. the air mass (see Fig. 1), gives rise to the Cartesian *incidence angles* (also called *wind angles*), which are the pitch-plane angle of attack α and yaw-plane sideslip angle β.

The wind frame relates "the velocity vector of the CM w.r.t. the air mass" to the body frame. In order to relate the "ground (inertial) velocity vector of the CM w.r.t. the Earth" (that is, velocity vector of the CM w.r.t. the air mass + wind velocity w.r.t. inertial fixed-Earth frame) to the inertial fixed-Earth frame, an additional frame is introduced, called the *velocity frame* $\mathcal{F}_V$ (also known as the *flight path frame*). Since air is at rest by Assumption A3, the two velocity vectors are in fact one and the same, so that the X_V coordinate axis also lies along the total velocity vector $\mathbf{V}$ of the vehicle CM, as shown in Fig. 1. Two angles γ and χ then describe the instantaneous angular orientation of the velocity coordinates relative to the Earth coordinate system. The horizontal flight path angle (or heading angle) χ is measured from North to the projection of $\mathbf{V}$ into the local tangent plane $X_E Y_E$ (positive clockwise about downward vertical Z_E), such that North and East are expressed by 0 and $\pi/2$ rad, respectively. The vertical flight path angle γ takes this projection vertically up to $\mathbf{V}$. Note that only X_W of wind coordinates has been defined without ambiguity, and so its orientation is now defined relative to velocity coordinates through the bank (roll) angle μ. The wind and velocity coordinates are then related through μ about the velocity vector, such that the velocity frame $\mathcal{F}_V$ is obtained by rotating $\mathcal{F}_W$ about the X_W axis so that the Y_V axis of $\mathcal{F}_V$ becomes parallel to the horizontal plane of $\mathcal{F}_E$.

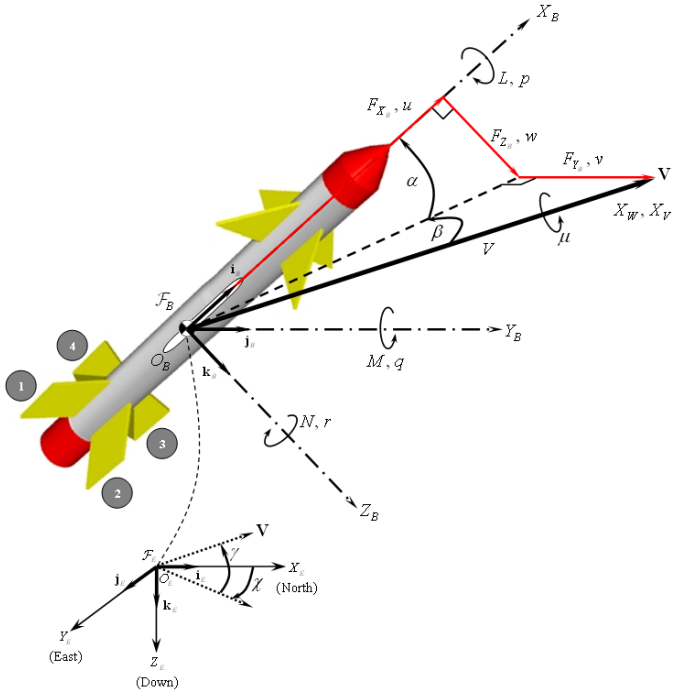

Fig. 1: Fixed-Earth and body-fixed reference frames showing vector components resolved in Cartesian body coordinates

Table 1: Nomenclature for vector components resolved in $\mathcal{F}_b$

Vector Symbol	Description	Units	Roll Axis O_BX_B	Pitch Axis O_BY_B	Yaw Axis O_BZ_B
$\mathbf{F}$	Total Force	N	F_{X_B}	F_{Y_B}	F_{Z_B}
$\mathbf{M}$	Total Moment	Nm	L	M	N
$\mathbf{V}$	Linear Velocity	ms^{-1}	u	v	w
$\boldsymbol{\omega}_{B/E}$	Angular Velocity	$rads^{-1}$	p	q	r
$\mathbf{a}$	Total Acceleration	ms^{-2}	a_{X_B}	a_{Y_B}	a_{Z_B}

2.2 Coordinate Transformations

Fig. 2 summarizes the different coordinate systems defined in Section 2.1, and depicts the transformation angles that relate them to each other. Now, let us present the orthonormal transformations that connect all these coordinate systems.

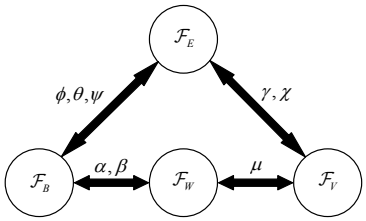

Fig. 2: Coordinate systems and transformation angles

The Euler angles ϕ, θ, and ψ relate the body coordinates to the Earth coordinates. The coordinate (or component) transformation matrix of body w.r.t. inertial coordinates is obtained using a 3-2-1 (yaw-pitch-roll) Euler sequence, giving

$$\mathbf{T}^{(B,E)} = \begin{bmatrix} 1 & 0 & 0 \\ 0 & \mathrm{c}_\phi & \mathrm{s}_\phi \\ 0 & -\mathrm{s}_\phi & \mathrm{c}_\phi \end{bmatrix} \begin{bmatrix} \mathrm{c}_\theta & 0 & -\mathrm{s}_\theta \\ 0 & 1 & 0 \\ \mathrm{s}_\theta & 0 & \mathrm{c}_\theta \end{bmatrix} \begin{bmatrix} \mathrm{c}_\psi & \mathrm{s}_\psi & 0 \\ -\mathrm{s}_\psi & \mathrm{c}_\psi & 0 \\ 0 & 0 & 1 \end{bmatrix}, \tag{1}$$

with $\mathrm{s}_{(\cdot)}$ and $\mathrm{c}_{(\cdot)}$ denoting shorthand notations for $\sin(\cdot)$ and $\cos(\cdot)$, respectively.

The orientation of body coordinates relative to wind coordinates is related through the angle of attack α and sideslip angle β. By noting that the wind coordinates are a transformation of the body coordinates using negative β and positive α rotation sequence, the transformation matrix $\mathbf{T}^{(B,W)}$ of body coordinates w.r.t. wind coordinates becomes

$$\mathbf{T}^{(B,W)} = \begin{bmatrix} \mathrm{c}_\alpha & 0 & -\mathrm{s}_\alpha \\ 0 & 1 & 0 \\ s_\alpha & 0 & c_\alpha \end{bmatrix} \begin{bmatrix} \mathrm{c}_\beta & -s_\beta & 0 \\ \mathrm{s}_\beta & c_\beta & 0 \\ 0 & 0 & 1 \end{bmatrix}. \tag{2}$$

The orientation of wind coordinates relative to velocity coordinates is related through the bank angle μ. The transformation matrix $\mathbf{T}^{(W,V)}$ of wind coordinates w.r.t. velocity coordinates is given by

$$\mathbf{T}^{(W,V)} = \begin{bmatrix} 1 & 0 & 0 \\ 0 & \mathrm{c}_\mu & \mathrm{s}_\mu \\ 0 & -\mathrm{s}_\mu & \mathrm{c}_\mu \end{bmatrix}. \tag{3}$$

Finally, the sequence of rotations χ and γ relate velocity coordinates to Earth coordinates, giving

$$\mathbf{T}^{(V,E)} = \begin{bmatrix} \mathrm{c}_\gamma & 0 & -\mathrm{s}_\gamma \\ 0 & 1 & 0 \\ \mathrm{s}_\gamma & 0 & \mathrm{c}_\gamma \end{bmatrix} \begin{bmatrix} \mathrm{c}_\chi & \mathrm{s}_\chi & 0 \\ -\mathrm{s}_\chi & \mathrm{c}_\chi & 0 \\ 0 & 0 & 1 \end{bmatrix}. \tag{4}$$

2.3 Translational Motion

The three translational degrees of freedom are governed by Newton's second law. Frequently, the trajectory of a vehicle is so slow compared to orbital speed and so close to the Earth that, under the nonrotating (stationary) and flat Earth Assumption A2, the Coriolis and centrifugal accelerations related to the rotation of the Earth and the changes in the direction of gravity as the missile moves over the surface of the Earth can be neglected. Then, under Assumption A2, the translational equations of motion of a flight vehicle over a nonrotating and flat Earth take on the vector form

$$d_E\mathbf{V}/dt = d_B\mathbf{V}/dt + \boldsymbol{\omega}_{B/E} \times \mathbf{V} = \mathbf{F}/m(t), \tag{5}$$

where $m(t)$ is the vehicle (variable) mass, $\mathbf{V}$ is the linear velocity vector of the missile CM w.r.t. to the Earth, $d_E\mathbf{V}/dt$ and $d_B\mathbf{V}/dt$ are its Earth-frame and body-frame derivatives, respectively, $\boldsymbol{\omega}_{B/E}$ is the angular velocity of $\mathcal{F}_B$ w.r.t. to $\mathcal{F}_E$, and $\mathbf{F}$ represents the vector sum of external forces applied directly to the missile, such that the acceleration of the missile CM w.r.t. to the Earth is given by $\mathbf{a} = d_E\mathbf{V}/dt = \mathbf{F}/m$.

Note that the mass is not constant in a missile during the operation of the propulsion system because of the consumption of propellant. It can be shown that (5) is applicable to a missile that has *variable mass* due to the burning of propellant if the value of m to be used in (5) is a function of time t. A derivation that rigorously takes into account the change in mass, and arrives at the same result for constant mass, except that m is now a function of time, is given in Meriam & Kraige (1986).

The vector differential equation (5), although valid in any reference frame, is simple enough to be expressed in the body frame $\mathcal{F}_B$ by resolving it into Cartesian body coordinates. Thus, using the vector components of $\mathbf{V}$, $\boldsymbol{\omega}_{B/E}$ and $\mathbf{F}$ in $\mathcal{F}_B$ defined in Table 1, yields the scalar equations for $d_B\mathbf{V}^{(B)}/dt$:

$$\left.\begin{aligned} \dot{u} &= rv - qw + F_{X_B}/m \\ \dot{v} &= pw - ru + F_{Y_B}/m \\ \dot{w} &= qu - pv + F_{Z_B}/m. \end{aligned}\right\} \tag{6}$$

The three first-order differential equations (6) govern the dynamics of the 3-DOF translational motions of a vehicle expressed in the body frame with the Earth as the inertial reference frame. These equations are nonlinear and coupled by the body rates $\boldsymbol{\omega}_{B/E}^{(B)} = [p \quad q \quad r]^T$. The nonlinearity enters through incidence angles in aerodynamic force and moment calculations (discussed later in Sections 2.5, 2.6 and 3.1).

2.4 Rotational Motion

The three rotational degrees of freedom are governed by Euler's law. The rotational equations of motion of a flight vehicle w.r.t. a nonrotating and flat Earth (Assumption A2) are expressed by the vector differential equation

$$\dot{\boldsymbol{\omega}}_{B/E} = \mathbf{I}^{-1}(t)\left(\mathbf{M} - \boldsymbol{\omega}_{B/E} \times \mathbf{I}(t)\boldsymbol{\omega}_{B/E}\right), \tag{7}$$

where $\mathbf{I}(t)$ is the (variable) inertia matrix of missile body referred to the CM, $\mathbf{I}\boldsymbol{\omega}_{B/E}$ is the angular momentum of body w.r.t. the Earth frame referred to the CM, and $\mathbf{M}$ represents the vector sum of all the external moments referred to the missile CM. Although the vector differential equation (7) is also valid in any reference frame, the body coordinates express the inertia matrix $\mathbf{I}$ in constant form, defined as

$$\mathbf{I}^{(B)} = \begin{bmatrix} I_x & -I_{xy} & -I_{xz} \\ -I_{xy} & I_y & -I_{yz} \\ -I_{xz} & -I_{yz} & I_z \end{bmatrix}, \tag{8}$$

which is a symmetric and positive-definite (nonsingular) matrix whose elements consist of the moments of inertia I_x, I_y, I_z about the axes of $\mathcal{F}_B$, and the products of inertia I_{xy}, I_{yz}, I_{xz} over the planes of $\mathcal{F}_B$, all having SI units of $\mathrm{kg\,m^2}$. Since the reference frame is fixed to the body, the inertia matrix appears constant in $\mathcal{F}_B$, and does not change by body motion. Note, however, that during the operation of the missile propulsion system, there is another source of change in the inertia matrix that is not related to body motion. As the propellant mass is expelled from the missile, the inertia matrix changes. Therefore, similar to the variable mass m, the parameter $\mathbf{I}$ is not constant in a missile during the operation of the propulsion system because of the consumption of propellant. Although a rigorous accounting for a variable inertia matrix is not easy, the time rate of change of $\mathbf{I}$ due to the burning of propellant is usually small enough that terms expressing this rate can be neglected. By this assumption, (7)

is also applicable to a missile that has variable inertia matrix, again provided that the value of $\mathbf{I}$ to be used in (7) is a function of time t.

Often, because of symmetry, missiles have body axes that coincide with the principal axes of the moment of inertias, and the inertia matrix exhibits only diagonal elements, which greatly simplifies the equations of motion, since the products-of-inertia terms vanish. Moreover, the mass distribution of a missile about its Y_B-axis is often essentially the same as that about its Z_B-axis. This is a particularly important case for conventional missiles having tetragonal symmetry that skid to turn, and manifest two equal principal moment of inertias. Therefore, the further simplification of setting $I_{yy} = I_{zz}$ is often possible; however, the distinction is retained here for generality. On the other hand, bank-to-turn or cruise missiles have aircraft-like symmetries, where all of the principal moment of inertia axes are not aligned with the body axes. However, due to the planar symmetry w.r.t. the X_B and Z_B axes (that is, $I_{xy} = I_{yz} = 0$), the Y_B axis is indeed a principal axis. Such a configuration gives rise to an inertia matrix in body coordinates with diagonal elements consisting of axial moments of inertia I_{xx} and I_{zz}, and the principal moment of inertia I_{yy}, and one off-diagonal element I_{xz}, leading to more complex solutions. Since the product-of-inertia term I_{xz}, in general, is nonzero, it is retained in the development of the rotational equations of motion.

For missiles with planar symmetry only in the X_BZ_B plane, there are four zero elements in the inertia matrix (8), so that its inversion can be tolerated, making it possible to solve for the body rate components $\boldsymbol{\omega}_{B/E}^{(B)} = [p \quad q \quad r]^T$ explicitly as scalar equations. The rates of change of the body rate components are thus obtained in scalar form by expressing (7) in the body frame $\mathcal{F}_B$, giving

$$\left.\begin{aligned}
\dot{p} &= \tfrac{1}{I_xI_z - I_{xz}^2}\left\{I_zL + I_{xz}N + [I_z(I_y - I_z) - I_{xz}^2]qr + I_{xz}(I_x - I_y + I_z)pq\right\} \\
\dot{q} &= \tfrac{1}{I_y}\left\{M + (I_z - I_x)pr - I_{xz}(p^2 - r^2)\right\} \\
\dot{r} &= \tfrac{1}{I_xI_z - I_{xz}^2}\left\{I_{xz}L + I_xN + [I_x(I_x - I_y) + I_{xz}^2]pq + I_{xz}(I_y - I_z - I_x)qr\right\}.
\end{aligned}\right\} \quad (9)$$

The three first-order differential equations (9) govern the dynamics of the 3-DOF rotational motions of a vehicle w.r.t. the inertial frame expressed in body axes. These equations are nonlinear and couple with the translational equations (6) only through the aerodynamic moments, which are contained in the total moments $\mathbf{M}^{(B)} = [L \quad M \quad N]^T$. Their integration yields the angular velocity of the body w.r.t. the inertial frame expressed in body coordinates, in short, the body rates $\boldsymbol{\omega}_{B/E}^{(B)} = [p \quad q \quad r]^T$.

Clearly, the product of inertia I_{xz} couples the pitch and yaw rates to the roll degrees of freedom, and a strong coupling exists for large values of I_{xz}. The pitch and yaw equations exhibit similar trends. Other phenomena caused by I_{xz} are the coupling of the yawing moment N into the roll axis and the rolling moment L into the yaw axis. Therefore, if $I_{xz} = 0$, as is the case for missiles with tetragonal symmetry, the rotational equations of motion (9) are greatly simplified.

2.5 Incidence Angles

The transformation of the missile velocity vector from relative wind coordinates to body coordinates is obtained from

$$\mathbf{V}^{(B)} = \mathbf{T}^{(B,W)}\mathbf{V}^{(W)}, \quad (10)$$

where $\mathbf{V}^{(B)} = [u \quad v \quad w]^T$, $\mathbf{V}^{(W)} = [V \quad 0 \quad 0]^T$, and V is the airspeed, given by the magnitude of the missile velocity vector, such that

$$V^2 = u^2 + v^2 + w^2. \quad (11)$$

Using (2) and (10), the components of the total velocity vector in body coordinates are thus obtained as

$$u = V\,\mathrm{c}_\alpha\,\mathrm{c}_\beta, \quad v = V\,\mathrm{s}_\beta, \quad w = V\,\mathrm{s}_\alpha\,\mathrm{c}_\beta. \quad (12)$$

The definitions for the Cartesian incidence angles are derived from (12) in terms of the velocity components in body coordinates (u, v, w) and the relative wind axis component (airspeed V), given by the algebraic relationships

$$\alpha = \tan^{-1}\tfrac{w}{u}, \quad \beta = \sin^{-1}\tfrac{v}{V}. \quad (13)$$

2.6 Forces and Moments

Equations (6) and (9) express the translational and rotational equations of motion in body coordinates. With the exception of Assumptions A1-A4, these equations are perfectly general, that is, no simplifying assumptions have been used in their derivation. Solution of these equations of motion requires knowledge of the sum of the forces and the sum of the moments acting on the missile. The forces and moments are produced by *gravity*, *aerodynamics*, and *propulsion*. Since, by Assumption A4, missile CM and CG are the same point, the gravitational force does not cause any external moment about the CM. Consequently, gravity contributes only as external force acting on the missile body axes. Therefore, the forces and moments are generally composed of:

- gravitational forces,
- aerodynamic forces and moments, and
- propulsive thrust forces and any moment caused either by design (such as thrust vectoring and/or reaction jet controls) or by error (misalignment of the thrust).

The total force applied to the missile body, therefore, consists of gravitational, aerodynamic and propulsive forces $\mathbf{F}_g$, $\mathbf{F}_a$ and $\mathbf{F}_p$, respectively, whereas the total moment acting on the body generally consists of aerodynamic and propulsive moments $\mathbf{M}_a$ and $\mathbf{M}_p$, respectively, giving $\mathbf{F} = \mathbf{F}_g + \mathbf{F}_a + \mathbf{F}_p$ and $\mathbf{M} = \mathbf{M}_a + \mathbf{M}_p$.

In aerodynamically controlled missiles, propulsive thrust is usually designed to act through the missile CM, and thus produces no moment about the CM (that is, $\mathbf{M}_p = \mathbf{0}$). When the thrust vector does not pass through the CM, either by design or error, the equations used to describe the resulting propulsive moment $\mathbf{M}_p$ on the missile is equal to the product of the magnitude of the thrust and the perpendicular distance between the thrust vector and the CM. In this study, only the generic design approach for aerodynamically controlled missiles will be developed in order to highlight the steps involved in the missile autopilot design procedure, without further complicating the nonlinear equations of motion. However, the formulation presented here can readily be extended to combining thrust vectoring and reaction jets into missiles' aerodynamic control system.

The flat-Earth model is represented by having the gravitational force always pointing along the Z_E axis in the inertial coordinate system, such that $\mathbf{g}^{(E)}$ is formulated in the form $[0 \quad 0 \quad g]^T$, where g is the acceleration due to gravity. Hence, gravity in body coordinates is modeled as $\mathbf{g}^{(B)} = \mathbf{T}^{(B,E)}\mathbf{g}^{(E)}$, using the transformation matrix $\mathbf{T}^{(B,E)}$ given

in (1). The gravitational force acting on the body can then be obtained from $\mathbf{F}_g^{(B)} = m\mathbf{g}^{(B)}$. The components of gravitational force resolved into body coordinates are thus obtained as

$$\mathbf{F}_g^{(B)} = mg[-\mathrm{s}_\theta \quad \mathrm{s}_\phi \mathrm{c}_\theta \quad \mathrm{c}_\phi \mathrm{c}_\theta]^T. \tag{14}$$

Aerodynamic forces and moments acting on the body are expressed in body coordinates using the nondimensional aerodynamic (axial, side and normal) body-axes force coefficients $C_X(-C_A)$, C_Y, $C_Z(-C_N)$, nondimensional aerodynamic (rolling, pitching and yawing) body-axes moment coefficients $C_{l_{CG}}$, $C_{m_{CG}}$, $C_{n_{CG}}$ acting about the CG, the dynamic pressure $\bar{q}$, missile reference (characteristic) length d (such as maximum diameter), and missile reference area S (such as maximum cross-sectional area), as follows:

$$\mathbf{F}_a^{(B)} = \bar{q}S[C_X \quad C_Y \quad C_Z]^T, \quad \mathbf{M}_a^{(B)} = \bar{q}Sd[C_{l_{CG}} \quad C_{m_{CG}} \quad C_{n_{CG}}]^T. \tag{15}$$

The dynamic pressure $\bar{q}$ is a function of airspeed V and air density ρ (which, in turn, is a function of the altitude h), and is obtained from

$$\bar{q} = \tfrac{1}{2}\rho V^2. \tag{16}$$

Since, by assumption, the thrust vector $\mathbf{F}_p$ passes along the X_B axis and through the missile CM, $\mathbf{F}_p$ does not create any external moment, giving

$$\mathbf{F}_p^{(B)} = [T \quad 0 \quad 0]^T, \quad \mathbf{M}_p^{(B)} = [0 \quad 0 \quad 0]^T. \tag{17}$$

The total forces and moments acting on the body can now be obtained from (14)-(17), which are expressed in component form in body coordinates as

$$\mathbf{F}^{(B)} = \begin{bmatrix} F_{X_B} \\ F_{Y_B} \\ F_{Z_B} \end{bmatrix} = \begin{bmatrix} -mg\,\mathrm{s}_\theta + \bar{q}SC_X + T \\ mg\,\mathrm{s}_\phi\,\mathrm{c}_\theta + \bar{q}SC_Y \\ mg\,\mathrm{c}_\phi\,\mathrm{c}_\theta + \bar{q}SC_Z \end{bmatrix}, \quad \mathbf{M}^{(B)} = \begin{bmatrix} L \\ M \\ N \end{bmatrix} = \begin{bmatrix} \bar{q}SdC_{l_{CG}} \\ \bar{q}SdC_{m_{CG}} \\ \bar{q}SdC_{n_{CG}} \end{bmatrix}. \tag{18}$$

Aerodynamic forces and moments are modeled directly in the body axes, using body-axes aerodynamic force and moment coefficients. These coefficients are typically functions of flight conditions, such as Mach number (M), altitude (h), incidence angles (α, β) and their rates ($\dot{\alpha}$, $\dot{\beta}$), body angular rates (p, q, r), effective (virtual) aerodynamic control surface deflections (δ_a, δ_e, δ_r), changes in CG, and whether the thrust power is on or off (referred to as plume effects). Thus,

$$\begin{aligned} &C_j = C_j(M, h, \alpha, \beta, \dot{\alpha}^*, \dot{\beta}^*, p^*, q^*, r^*, \delta_a, \delta_e, \delta_r, \text{CG, thrust on/off}), \\ &j = X, Y, Z, l_{CG}, m_{CG}, n_{CG}, \quad (\cdot)^* = \tfrac{d}{2V}(\cdot), \end{aligned} \tag{19}$$

with $(\cdot)^*$ representing nondimensionalized motion related variables for angular rates. These complicated and highly nonlinear functions are used in the equations of motion to model the airframe's aerodynamics. Note that, since all coefficients are unitless, all angles are in radians. Note also that the control surface deflections can be canard, wing or tail.

3. DERIVATION OF THE NONLINEAR DYNAMIC EQUATIONS FOR MISSILE AUTOPILOT DESIGN

With the general equations of motion of a flight vehicle over a flat Earth in place, we can now proceed with the first step necessary for autopilot development. This will be deriving the equations of motion required for nonlinear missile autopilot design, which is pursued for all variables used in the aerodynamic coefficients. Since aerodynamic coefficients for missiles are generally modeled as having functional dependence on several variables given in (19), the equations of motion for autopilot design will be developed based on at least these variables, in addition to the command variables that will be conveyed to the autopilot.

3.1 Aerodynamic Model

In this work, a generic and realistic aerodynamic model, applicable as a general rule to missiles, is proposed. Because of the complicated functional dependence of the aerodynamic coefficients represented in (19), in practice, each "total" coefficient is modeled as the sum of a *baseline component* (that are, individually, functions of fewer variables), plus *incremental terms*. The baseline components are primarily functions of M, α, β, δ_a, δ_e, δ_r, whereas incremental terms are functions of only M. Component buildups of the "total" nondimensional aerodynamic coefficients for missiles, in general, are then expressed in the form

$$\left.\begin{aligned} C_X &= C'_{X_j}(M, h, \alpha, \beta, \delta_a, \delta_e, \delta_r) \text{ for } j = \text{thrust on/off} \\ C_Y &= C'_Y(M, \alpha, \beta, \delta_r) + \tfrac{d}{2V}[C_{Y_r}(M)r + C_{Y_{p\alpha}}(M)p\alpha] \\ C_Z &= C'_Z(M, \alpha, \beta, \delta_e) + \tfrac{d}{2V}[C_{Z_q}(M)q + C_{Z_{\dot{\alpha}}}(M)\dot{\alpha} + C_{Y_{p\alpha}}(M)p\beta] \\ C_{l_{CG}} &= C'_{l_{RP}}(M, \alpha, \beta, \delta_a, \delta_e, \delta_r) + \tfrac{d}{2V}C_{l_p}(M)p \\ C_{m_{CG}} &= C'_{m_{RP}}(M, \alpha, \beta, \delta_e) - lC_Z + \tfrac{d}{2V}[C_{m_q}(M)q + C_{m_{\dot{\alpha}}}(M)\dot{\alpha} + C_{n_{p\alpha}}(M)p\beta] \\ C_{n_{CG}} &= C'_{n_{RP}}(M, \alpha, \beta, \delta_r) + lC_Y + \tfrac{d}{2V}[C_{n_r}(M)r + C_{n_{\dot{\beta}}}(M)\dot{\beta} + C_{n_{p\alpha}}(M)p\alpha], \end{aligned}\right\} \tag{20}$$

where all angular-rate variables are nondimensionalized. The baseline components are the first terms on the right-hand side of the equations, which are followed by incremental terms, in the order of importance, consisting of the angular-rate variables. The coefficients of these incremental terms, indicated by an additional level of subscripts, represent *aerodynamic derivatives*, which are partial derivatives of the aerodynamic force and moment coefficients, all having functional dependence on the Mach number M. Note that the Magnus terms $C_{Y_{p\alpha}}$ and $C_{n_{p\alpha}}$ in (20) are particularly significant for agile missiles with canard-controlled and rolling airframe configurations, in which case they should be included in the autopilot model (Nielsen, 1988).

Due to the significant changes in CG position during propellant consumption, aerodynamic rolling, pitching and yawing moments are generally measured about a fixed *reference point* (RP) at a distance of x_{RP} meters from the missile nose (in the case the reference point is the missile nose, then $x_{RP} = 0$), thus obtaining $C_{l_{RP}}$, $C_{m_{RP}}$ and $C_{n_{RP}}$. In this way, the implicit dependence of the aerodynamic moment coefficients on the varying CG position is avoided. The moment coefficients about the CG ($C_{l_{CG}}$, $C_{m_{CG}}$ and $C_{n_{CG}}$) are then obtained by shifting moments about the fixed RP to the instantaneous CG position, located x_{CG} meters away from missile nose, using the moment arm $x_{CG} - x_{RP}$. Although this is assumed to have no effect on $C_{l_{CG}}$ ($C_{l_{CG}} = C_{l_{RP}}$), the shifting of aerodynamic moments from the RP to the CG couples C_Z into $C_{m_{CG}}$ and C_Y into $C_{n_{CG}}$, as is evident from the latter two expressions in (20), where $l \triangleq (x_{CG} - x_{RP})/d$. In doing so, the dependence of these coefficients on the instantaneous CG position, which varies during propellant consumption, is explicitly expressed.

Data for baseline components and incremental terms in (20) are derived from empirical methods, aerodynamic prediction programs, computational modeling, and/or through wind-tunnel experiments, and are compiled in the aerodynamic database generally in the form of look-up tables. Incremental terms consist of 1-dimensional look-up tables, since these are functions of only the Mach number. However, look-up tables for baseline components are necessarily multi-dimensional.

For the development of the autopilot model, general nonlinear representations of baseline components will now be presented. The proposed model uses nonlinear representations *up to cubic terms* for baseline components of "total" aerodynamic force and moment coefficients, and captures the most significant nonlinearities attributed to missiles, as follows:

$$\left.\begin{aligned}
C'_{X_j} &= C_{X_0} + a_1\alpha^2 + a_2\beta^2 + a_3\alpha\delta_e + a_4\beta\delta_r + a_5\delta_e^{\,2} + a_6\delta_r^{\,2} + a_7\delta_a^{\,2} \\
C'_Y &= C_{Y_0} + C_{Y_{\delta_r}}\delta_r + b_1\beta + b_2\beta^2 + b_3|\beta|\beta + b_4\beta^3 + b_5\alpha^2\beta \\
C'_Z &= C_{Z_0} + C_{Z_{\delta_e}}\delta_e + c_1\alpha + c_2\alpha^2 + c_3|\alpha|\alpha + c_4\alpha^3 + c_5\alpha\beta^2 \\
C'_{l_{RP}} &= C_{l_0} + d_1\delta_a + d_2\alpha^2\delta_a + d_3\beta^2\delta_a + d_4\alpha\delta_e + d_5\beta\delta_r \\
C'_{m_{RP}} &= C_{m_0} + C_{m_{\delta_e}}\delta_e + e_1\alpha + e_2\alpha^2 + e_3|\alpha|\alpha + e_4\alpha^3 + e_5\alpha\beta^2 \\
C'_{n_{RP}} &= C_{n_0} + C_{n_{\delta_r}}\delta_r + f_1\beta + f_2\beta^2 + f_3|\beta|\beta + f_4\beta^3 + f_5\alpha^2\beta,
\end{aligned}\right\} \quad (21)$$

where the newly introduced aerodynamic derivatives (such as $C_{Y_{\delta_r}}$, $C_{Z_{\delta_e}}$, etc.) as well as the rest of the coefficients (such as a_1, b_1, etc.) in these expressions all have functional dependence on only the Mach number M, although not explicitly shown in (21) for notational convenience.

The proposed form of the aerodynamic coefficients given in (21) can be obtained using data fitting techniques. Noting that there is linearity with respect to the unknown coefficients of the baseline components in (21), *linear least squares* method can be used to estimate these parameters. The best fit to the tabulated aerodynamic data using the proposed model (21) is then obtained by solving the resulting overdetermined system. For example, suppose that the baseline component C'_Z is represented in tabular form as a function of only the three variables M, α and δ_e. Hence, from (21),

$$C'_Z = C_{Z_0}(M) + C_{Z_{\delta_e}}(M)\delta_e + c_1(M)\alpha + c_2(M)\alpha^2 + c_3(M)|\alpha|\alpha + c_4(M)\alpha^3,$$

which is a multinomial in two independent variables α and δ_e. Suppose also that C'_Z is tabulated, say, using x, y and z breakpoints of M, α and δ_e, respectively. This results in yz equations for 6 unknowns for each set of Mach breakpoints $k = 1, \ldots, x$, and yields an overdetermined system $\mathbf{A}_k\mathbf{x}_k = \mathbf{b}_k$, where $\mathbf{A}_k \in \mathbb{R}^{yz\times 6}$, $\mathbf{b}_k \in \mathbb{R}^{yz\times 1}$ and

$$\mathbf{x}_k = [C_{Z_0,k} \quad C_{Z_{\delta_e},k} \quad c_{1,k} \quad c_{2,k} \quad c_{3,k} \quad c_{4,k}]^T$$

with $yz \gg 6$. The best fit that gives the optimal parameter values $\hat{\mathbf{x}}_k$ is then found by solving the corresponding normal equation of the overdetermined system, that is, $(\mathbf{A}_k{}^T\mathbf{A}_k)\hat{\mathbf{x}}_k = \mathbf{A}_k{}^T\mathbf{b}_k$. This is carried out for the complete set of Mach breakpoints $k = 1, \ldots, x$. Then, if desired, the 6 coefficients solved at each Mach breakpoint can be obtained in analytical form as functions of Mach number, by fitting an appropriate function (such as polynomial, Fourier, etc.) to these data. Another option is to store these coefficients in 1-dimensional look-up tables and use interpolation techniques to obtain intermediate values online.

Nonlinear and coupled terms in (21) represent the dominant nonlinearities in the baseline components of the missile aerodynamic force and moment coefficients. Coupled terms in these expressions produce coupling between channels at high angle of attack. Depending on the application, some of these terms may have negligible effect on missile aerodynamics and, hence, may be neglected. For example, some of the terms at zero incidence angles and control deflections (C_{Y_0}, C_{Z_0}, C_{l_0}, C_{m_0}, C_{n_0}) will be zero, except for asymmetric airframes/ airfoils. Similarly, α^2 and β^2 terms in the expressions for C'_Y, C'_Z, C'_m and C'_n will be obtained as zero when data is symmetric w.r.t. the origin. However, these terms will not be zero for unsymmetrical data, in which case they must be retained. In addition, inclusion of second-order nonlinearities $|\alpha|\alpha$ and $|\beta|\beta$ in the expressions provides more accurate estimates to those obtained using α^3 and β^3 terms alone, respectively, and vice versa. Some of the neglected terms (such as higher order terms), on the other hand, are often negligible, but can be included in the expressions if desired.

3.2 Mach Dynamics

Aerodynamic coefficients are modeled as having functional dependence on the Mach number M, as opposed to body-axes components u, v, w or the airspeed V. A differential equation describing the dynamics of M is thus required, which can be derived from the algebraic relationship

$$M = V/a, \quad (22)$$

where a is the speed of sound. Assuming a standard atmospheric model, the speed of sound is a function of the altitude h. Thus, differentiating (22) gives

$$\dot{M} = \tfrac{\dot{V}a - V\dot{a}}{a^2}.$$

However, inside the troposphere (the lowest portion of the Earth's atmosphere, which extends from sea level up to 11 km), the speed of sound changes only around 10% in value. Therefore, even though h and a are both varying, the time rate of change of a is so small that, in the derivation of the differential equation for Mach number, it can be assumed zero, giving

$$\dot{M} \cong \dot{V}/a. \quad (23)$$

The equation for $\dot{V}$ is obtained by differentiating (11), and substituting (6) to give

$$\begin{aligned}
\dot{V} &= \tfrac{1}{V}(u\dot{u} + v\dot{v} + w\dot{w}) \\
&= \tfrac{1}{V}[u(a_{X_B} - qw + rv) + v(a_{Y_B} - ru + pw) + w(a_{Z_B} - pv + qu)],
\end{aligned}$$

where $a_{X_B} = F_{X_B}/m$, $a_{Y_B} = F_{Y_B}/m$, and $a_{Z_B} = F_{Z_B}/m$ are the components of total acceleration in body coordinates resulting from the *gravitational*, *aerodynamic* and *thrust* forces acting on the vehicle. Substituting (12) into this equation yields the differential equation for airspeed, that is,

$$\dot{V} = a_{X_B}\,\mathrm{c}_\alpha\,\mathrm{c}_\beta + a_{Y_B}\,\mathrm{s}_\beta + a_{Z_B}\,\mathrm{s}_\alpha\,\mathrm{c}_\beta. \quad (24)$$

Hence, substituting (24) into (23) yields

$$\dot{M} = \tfrac{1}{a}(a_{X_B}\,\mathrm{c}_\alpha\,\mathrm{c}_\beta + a_{Y_B}\,\mathrm{s}_\beta + a_{Z_B}\,\mathrm{s}_\alpha\,\mathrm{c}_\beta). \quad (25)$$

3.3 Incidence Angle Dynamics

Using body coordinates, the translational equations of motion (6) are solved for the rates of change of the components u, v and w of the total velocity vector $\mathbf{V}$. Their integration yields u, v and w, which are used to calculate α and β using (13). The use of the wind coordinate system causes the rate of change of the magnitude of the velocity vector (V) to also lie along the X_W wind axis, and yields explicit equations for the rates of change of α and β. The following derivation will form a set of differential equations describing the dynamics of α and β, valid for large α and $\beta < 90°$.

The equations for $\dot{\alpha}$ and $\dot{\beta}$ are obtained by differentiating (13) and using (12) to yield

$$\dot{\alpha} = \tfrac{u\dot{w} - w\dot{u}}{u^2 + w^2} = \tfrac{\dot{w}\,\mathrm{c}_\alpha - \dot{u}\,\mathrm{s}_\alpha}{V\,\mathrm{c}_\beta}, \quad \dot{\beta} = \tfrac{V\dot{v} - v\dot{V}}{V\sqrt{V^2 - v^2}} = \tfrac{\dot{v} - \dot{V}\,\mathrm{s}_\beta}{V\,\mathrm{c}_\beta}.$$

Substituting (6), (22) and (24) into these equations yields

$$\dot{\alpha} = q - (p\,\mathrm{c}_\alpha + r\,\mathrm{s}_\alpha)\,\mathrm{t}_\beta + \tfrac{1}{Ma\,\mathrm{c}_\beta}(a_{Z_B}\,\mathrm{c}_\alpha - a_{X_B}\,\mathrm{s}_\alpha) \qquad (26)$$

$$\dot{\beta} = p\,\mathrm{s}_\alpha - r\,\mathrm{c}_\alpha - \tfrac{1}{Ma}(a_{X_B}\,\mathrm{c}_\alpha\,\mathrm{s}_\beta - a_{Y_B}\,\mathrm{c}_\beta + a_{Z_B}\,\mathrm{s}_\alpha\,\mathrm{s}_\beta), \qquad (27)$$

where $\mathrm{t}_{(\cdot)}$ denotes $\tan(\cdot)$.

3.4 Actuator Dynamics

Missiles operate using four aerodynamic control surfaces, using either *canards* or *wings* or *tail fins*. Generally, these four control surfaces actuate independently, each driven by a separate but identical actuator (servomotor). These actuators are required for tracking the guidance commands (such as lateral and normal acceleration commands expressed in g's) through actual control surface deflections δ_i via commanded control surface deflections δ_i^{com}, with $i = 1, \ldots, 4$. Therefore, the *effective* (*virtual*) *control surface deflection* commands of *aileron* (roll), *elevator* (pitch), and *rudder* (yaw) control ($\delta_a, \delta_e, \delta_r$) from the missile autopilot are distributed to the four (*actual*) *individual control surface deflections* δ_i ($i = 1, \ldots, 4$). The control mixing logic that relates these effective control surface deflections to individual control surface deflections is configuration specific, and depends upon whether the missile flies with a "+" or "×" aerodynamic control (or "delta") configuration, as shown in Fig. 3. The arrows in this figure show the direction of forces and leading edge of panel where, by convention, a positive panel deflection is one which will produce a negative (counterclockwise when viewed from the rear) rolling moment increment at zero angle of attack and sideslip. The equations for the control surface mixing logic are then given by

$$[\delta_a \quad \delta_e \quad \delta_r]^T = \mathbf{\Delta}_{\text{logic}}[\delta_1 \quad \delta_2 \quad \delta_3 \quad \delta_4]^T. \qquad (28)$$

Two conventional mixing logics for the "+" and "×" delta configurations, respectively, are defined by

$$\mathbf{\Delta}^{+}_{\text{logic}} = \frac{1}{4}\begin{bmatrix} 1 & 1 & 1 & 1 \\ 0 & 2 & 0 & -2 \\ 2 & 0 & -2 & 0 \end{bmatrix}, \qquad \mathbf{\Delta}^{\times}_{\text{logic}} = \frac{1}{4}\begin{bmatrix} 1 & 1 & 1 & 1 \\ 1 & 1 & -1 & -1 \\ 1 & -1 & -1 & 1 \end{bmatrix}.$$

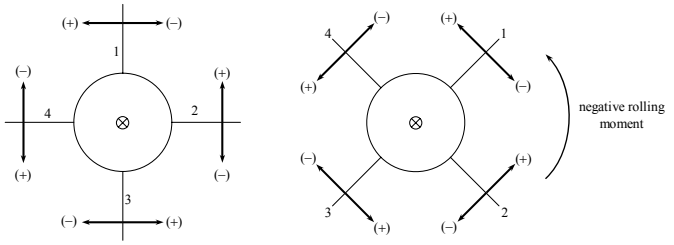

Fig. 3. Rear-View Projection of "+", "×" Delta Configurations

For satisfactory autopilot performance, actuator dynamics must also be considered. It is usually sufficient to consider a second-order actuator dynamic model, with transfer function

$$\frac{\delta_i(s)}{\delta_i^{com}(s)} = \frac{\omega_n^{\,2}}{s^2 + 2\zeta\omega_n s + \omega_n^{\,2}}, \quad i = 1, \ldots, 4,$$

where ζ is the actuator damping ratio, ω_n is the natural frequency, δ_i^{com} is the commanded control surface deflection of the i^{th} aerodynamic control surface, and δ_i is its actual deflection. However, actuators possess significant nonlinearities, such as angular position and rate limits as well as mechanical backlash, and it is preferable to include these nonlinearities in the actuator model. It is important to note that it is δ_i that exhibit these nonlinearities (not $\delta_a, \delta_e, \delta_r$).

In the design and the analysis of the nonlinear autopilot, actuator dynamics are modeled using *actuator saturation*, that is, *position and rate limits* of the aerodynamic control surfaces, as shown in Fig. 4. Actuator dynamics are, therefore, represented by the 2nd-order nonlinear differential equation

$$\ddot{\delta}_i = (\delta_i^{com} - \text{sat}(\delta_i, \delta_{\max}))\omega_n^{\,2} - 2\zeta\omega_n^{\,2}\,\text{sat}(\dot{\delta}_i, \dot{\delta}_{\max}) \qquad (29)$$

using the saturation function

$$\text{sat}(\sigma, \sigma_{\max}) \triangleq \begin{cases} \sigma_{\max}, & \sigma > \sigma_{\max} \\ \sigma, & |\sigma| \le \sigma_{\max} \\ -\sigma_{\max}, & \sigma < -\sigma_{\max} \end{cases}$$

with $\sigma = \delta_i, \dot{\delta}_i$, for $i = 1, \ldots, 4$.

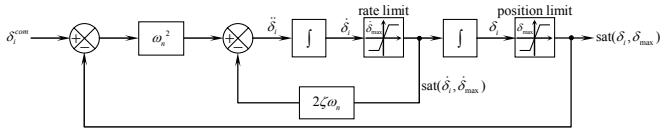

Fig. 4. 2nd-Order Nonlinear Actuator Block Diagram Model

Therefore, defining the actual and the commanded control surface deflection vectors, respectively, as

$$\boldsymbol{\delta} \triangleq [\delta_1 \quad \delta_2 \quad \delta_3 \quad \delta_4]^T$$

$$\boldsymbol{\delta}^{com} \triangleq [\delta_1^{com} \quad \delta_2^{com} \quad \delta_3^{com} \quad \delta_4^{com}]^T,$$

(29) can be represented in state-space form as

$$\begin{bmatrix} \dot{\boldsymbol{\delta}} \\ \ddot{\boldsymbol{\delta}} \end{bmatrix} = \begin{bmatrix} \mathbf{0}_{4\times4} & \mathbf{I}_{4\times4} \\ -\omega_n^{\,2}\,\text{diag}\left\{\frac{\text{sat}(\delta_i, \delta_{\max})}{\delta_i}\right\} & -2\zeta\omega_n^{\,2}\,\text{diag}\left\{\frac{\text{sat}(\dot{\delta}_i, \dot{\delta}_{\max})}{\dot{\delta}_i}\right\} \end{bmatrix}\begin{bmatrix} \boldsymbol{\delta} \\ \dot{\boldsymbol{\delta}} \end{bmatrix} + \begin{bmatrix} \mathbf{0}_{4\times4} \\ \omega_n^{\,2}\mathbf{I}_{4\times4} \end{bmatrix}\boldsymbol{\delta}^{com} \qquad (30)$$

for $i = 1, \ldots, 4$, where $\mathbf{0}_{4\times4}$ and $\mathbf{I}_{4\times4}$ are 4×4 zero and identity matrices, respectively, and $\text{diag}\{\cdot\}$ represents a diagonal matrix.

3.5 Body Rate Dynamics

Expanding the equations derived in (9), substituting the total moments (18) and aerodynamic coefficients (20)-(21), and using the derivations obtained for $\dot{\alpha}$ and $\dot{\beta}$ in (26) and (27), respectively, yields the following nonlinear representations for missile body angular rate dynamics:

$$\left.\begin{aligned} \dot{p} &= L_{bias} + L_p p + L_r r + L_{pq} pq + L_{qr} qr + L_{\delta_a}\delta_a + L_{\delta_e}\delta_e + L_{\delta_r}\delta_r \\ \dot{q} &= M_{bias} + M_p p + M_q q + M_r r + M_{p^2} p^2 + M_{r^2} r^2 + M_{pr} pr + M_{\delta_e}\delta_e \\ \dot{r} &= N_{bias} + N_p p + N_r r + N_{pq} pq + N_{qr} qr + N_{\delta_a}\delta_a + N_{\delta_e}\delta_e + N_{\delta_r}\delta_r \end{aligned}\right\} \qquad (31)$$

where the coefficients are defined as

$$L_{bias} \triangleq kI_z C_{l_0} + kI_{xz}[(C_{n_0} + lC_{Y_0}) + (f_1 + lb_1)\beta + (f_2 + lb_2)\beta^2 + (f_3 + lb_3)|\beta|\beta + (f_4 + lb_4)\beta^3 + (f_5 + lb_5)\alpha^2\beta - \tfrac{d}{2V}\tfrac{1}{Ma}(C_{n_\beta} + lC_{Y_\beta})(a_{X_B}\,\mathrm{c}_\alpha\,\mathrm{s}_\beta - a_{Y_B}\,\mathrm{c}_\beta + a_{Z_B}\,\mathrm{s}_\alpha\,\mathrm{s}_\beta)]$$

$$L_p \triangleq \tfrac{d}{2V}k[I_z C_{l_p} + I_{xz}(C_{n_{p\alpha}} + lC_{Y_{p\alpha}})\alpha + I_{xz}(C_{n_\beta} + lC_{Y_\beta})\,\mathrm{s}_\alpha]$$

$$L_r \triangleq \tfrac{d}{2V}kI_{xz}[(C_{n_r} + lC_{Y_r}) - (C_{n_{\dot{\beta}}} + lC_{Y_{\dot{\beta}}})\,\mathrm{c}_\alpha] \qquad L_{pq} \triangleq I_{xz}(I_x - I_y + I_z)\big/(I_x I_z - I_{xz}^{\,2})$$

$$L_{qr} \triangleq [I_z(I_y - I_z) - I_{xz}^{\,2}]\big/(I_x I_z - I_{xz}^{\,2}) \qquad L_{\delta_a} \triangleq kI_z(d_1 + d_2\alpha^2 + d_3\beta^2)$$

$$L_{\delta_e} \triangleq kI_z d_4\alpha \qquad L_{\delta_r} \triangleq k[I_z d_5\beta + I_{xz}(C_{n_{\delta_r}} + lC_{Y_{\delta_r}})]$$

$$M_{bias} \triangleq \tfrac{\bar{q}Sd}{I_y}[(C_{m_0} - lC_{Z_0}) + (e_1 - lc_1)\alpha + (e_2 - lc_2)\alpha^2 + (e_3 - lc_3)|\alpha|\alpha + (e_4 - lc_4)\alpha^3 + (e_5 - lc_5)\alpha\beta^2 + \tfrac{d}{2V}\tfrac{1}{Ma\,\mathrm{c}_\beta}(C_{m_\alpha} - lC_{Z_\alpha})(a_{Z_B}\,\mathrm{c}_\alpha - a_{X_B}\,\mathrm{s}_\alpha)]$$

$$M_p \triangleq \tfrac{\bar{q}Sd^2}{2VI_y}[(C_{n_{\dot{\alpha}r}} - lC_{Y_{\dot{\alpha}r}})\beta - (C_{m_{\dot{\alpha}}} - lC_{Z_{\dot{\alpha}}})\,\mathrm{c}_\alpha\,\mathrm{t}_\beta]$$

$$M_q \triangleq \tfrac{\bar{q}Sd^2}{2VI_y}[(C_{m_q} - lC_{Z_q}) + (C_{m_{\dot{\alpha}}} - lC_{Z_{\dot{\alpha}}})] \qquad M_r \triangleq -\tfrac{\bar{q}Sd^2}{2VI_y}(C_{m_{\dot{\alpha}}} - lC_{Z_{\dot{\alpha}}})\,\mathrm{s}_\alpha\,\mathrm{t}_\beta$$

$$M_{p^2} \triangleq -I_{xz}\big/I_y \qquad M_{r^2} \triangleq I_{xz}\big/I_y$$

$$M_{pr} \triangleq (I_z - I_x)\big/I_y \qquad M_{\delta_e} \triangleq \tfrac{\bar{q}Sd}{I_y}(C_{m_{\delta_e}} - lC_{Z_{\delta_e}})$$

$$N_{bias} \triangleq kI_{xz}C_{l_0} + kI_x[(C_{n_0} + lC_{Y_0}) + (f_1 + lb_1)\beta + (f_2 + lb_2)\beta^2 + (f_3 + lb_3)|\beta|\beta + (f_4 + lb_4)\beta^3 + (f_5 + lb_5)\alpha^2\beta - \tfrac{d}{2V}\tfrac{1}{Ma}(C_{n_\beta} + lC_{Y_\beta})(a_{X_B}\,\mathrm{c}_\alpha\,\mathrm{s}_\beta - a_{Y_B}\,\mathrm{c}_\beta + a_{Z_B}\,\mathrm{s}_\alpha\,\mathrm{s}_\beta)]$$

$$N_p \triangleq \tfrac{d}{2V}k[I_{xz}C_{l_p} + I_x(C_{n_{p\alpha}} + lC_{Y_{p\alpha}})\alpha + I_x(C_{n_\beta} + lC_{Y_\beta})\,\mathrm{s}_\alpha]$$

$$N_r \triangleq \tfrac{d}{2V}kI_x[(C_{n_r} + lC_{Y_r}) - (C_{n_{\dot{\beta}}} + lC_{Y_{\dot{\beta}}})\,\mathrm{c}_\alpha] \qquad N_{pq} \triangleq [I_x(I_x - I_y) + I_{xz}^{\,2}]\big/(I_x I_z - I_{xz}^{\,2})$$

$$N_{qr} \triangleq I_{xz}(I_y - I_z - I_x)\big/(I_x I_z - I_{xz}^{\,2}) \qquad N_{\delta_a} \triangleq kI_{xz}[d_1 + d_2\alpha^2 + d_3\beta^2]$$

$$N_{\delta_e} \triangleq kI_{xz}d_4\alpha \qquad N_{\delta_r} \triangleq k[I_{xz}d_5\beta + I_x(C_{n_{\delta_r}} + lC_{Y_{\delta_r}})]$$

which are highly nonlinear functions of $M, \alpha, \beta, \dot{\alpha}, \dot{\beta}, V$, with $k \triangleq \bar{q}Sd/(I_x I_z - I_{xz}^2)$, $\bar{q} = \frac{1}{2}\rho V^2$ and $l = (x_{cg} - x_{ref})/d$. Although not explicitly shown, recall that the moment and product of inertia terms in these expressions are time-varying due to changes in CG position during propellant consumption.

3.6 Acceleration Dynamics

First, a relation between the Euler angular rates $\dot{\phi}, \dot{\theta}, \dot{\psi}$ and the body-fixed angular rates $\boldsymbol{\omega}_{B/E}^{(B)} = [p \quad q \quad r]^T$ is required. Using a ψ-θ-ϕ rotation sequence from fixed-Earth coordinates to body-fixed coordinates and then inverting this matrix equation yields

$$\begin{bmatrix} p \\ q \\ r \end{bmatrix} = \begin{bmatrix} 1 & 0 & -\mathrm{s}_\theta \\ 0 & \mathrm{c}_\phi & \mathrm{s}_\phi \mathrm{c}_\theta \\ 0 & -\mathrm{s}_\phi & \mathrm{c}_\phi \mathrm{c}_\theta \end{bmatrix} \begin{bmatrix} \dot{\phi} \\ \dot{\theta} \\ \dot{\psi} \end{bmatrix} \quad \Rightarrow \quad \begin{bmatrix} \dot{\phi} \\ \dot{\theta} \\ \dot{\psi} \end{bmatrix} = \begin{bmatrix} 1 & \mathrm{s}_\phi \mathrm{t}_\theta & \mathrm{c}_\phi \mathrm{t}_\theta \\ 0 & \mathrm{c}_\phi & -\mathrm{s}_\phi \\ 0 & \mathrm{s}_\phi/\mathrm{c}_\theta & \mathrm{c}_\phi/\mathrm{c}_\theta \end{bmatrix} \begin{bmatrix} p \\ q \\ r \end{bmatrix}.$$

Let us now derive the rigid-body acceleration dynamics for the missile body acceleration components at the CM. The components of acceleration in body coordinates, $\mathbf{a}^{(B)} = [a_{X_B} \quad a_{Y_B} \quad a_{Z_B}]^T$, are obtained from the components of total force acting at the CM along the missile body coordinate axes, $\mathbf{F}^{(B)} = [F_{X_B} \quad F_{Y_B} \quad F_{Z_B}]^T$, divided by the mass m. Now, taking into account the dependence of $\bar{q}$ on V in (16), and recalling the functional dependence of the aerodynamic force coefficients on flight conditions α, β and the aerodynamic control surfaces $\delta_a, \delta_e, \delta_r$, differentiating $\mathbf{a}^{(B)} = \mathbf{F}^{(B)}/m$ using (18), keeping terms up to first order, ignoring the time rate of change of thrust, substituting for the Euler angular rates, and grouping terms yields the acceleration dynamics

$$\begin{bmatrix} \dot{a}_{X_B} \\ \dot{a}_{Y_B} \\ \dot{a}_{Z_B} \end{bmatrix} = g \begin{bmatrix} 0 & -\mathrm{c}_\phi \mathrm{c}_\theta & \mathrm{s}_\phi \mathrm{c}_\theta \\ \mathrm{c}_\phi \mathrm{c}_\theta & 0 & \mathrm{s}_\theta \\ -\mathrm{s}_\phi \mathrm{c}_\theta & -\mathrm{s}_\theta & 0 \end{bmatrix} \begin{bmatrix} p \\ q \\ r \end{bmatrix} + \tfrac{1}{m}\bar{q}S \left(\begin{bmatrix} \partial C_X & C_{X_\alpha} & C_{X_\beta} \\ \partial C_Y & C_{Y_\alpha} & C_{Y_\beta} \\ \partial C_Z & C_{Z_\alpha} & C_{Z_\beta} \end{bmatrix} \begin{bmatrix} \dot{V} \\ \dot{\alpha} \\ \dot{\beta} \end{bmatrix} + \begin{bmatrix} C_{X_{\delta_a}} & C_{X_{\delta_e}} & C_{X_{\delta_r}} \\ C_{Y_{\delta_a}} & C_{Y_{\delta_e}} & C_{Y_{\delta_r}} \\ C_{Z_{\delta_a}} & C_{Z_{\delta_e}} & C_{Z_{\delta_r}} \end{bmatrix} \begin{bmatrix} \dot{\delta}_a \\ \dot{\delta}_e \\ \dot{\delta}_r \end{bmatrix} \right).$$

Substituting (22), (24), (26) and (27) into this equation, the acceleration dynamics can be represented in the compact form

$$\begin{aligned} \begin{bmatrix} \dot{a}_{X_B} \\ \dot{a}_{Y_B} \\ \dot{a}_{Z_B} \end{bmatrix} &= \tfrac{1}{mMa}\bar{q}S \begin{bmatrix} \partial_{Ma} C_X & C_{X_\alpha} & C_{X_\beta} \\ \partial_{Ma} C_Y & C_{Y_\alpha} & C_{Y_\beta} \\ \partial_{Ma} C_Z & C_{Z_\alpha} & C_{Z_\beta} \end{bmatrix} \begin{bmatrix} Ma\,\mathrm{c}_\alpha \mathrm{c}_\beta & Ma\,\mathrm{s}_\beta & Ma\,\mathrm{s}_\alpha \mathrm{c}_\beta \\ -\mathrm{s}_\alpha/\mathrm{c}_\beta & 0 & \mathrm{c}_\alpha/\mathrm{c}_\beta \\ -\mathrm{c}_\alpha \mathrm{s}_\beta & \mathrm{c}_\beta & -\mathrm{s}_\alpha \mathrm{s}_\beta \end{bmatrix} \begin{bmatrix} a_{X_B} \\ a_{Y_B} \\ a_{Z_B} \end{bmatrix} \\ &+ \tfrac{1}{m}\bar{q}S \begin{bmatrix} \partial_{Ma} C_X & C_{X_\alpha} & C_{X_\beta} \\ \partial_{Ma} C_Y & C_{Y_\alpha} & C_{Y_\beta} \\ \partial_{Ma} C_Z & C_{Z_\alpha} & C_{Z_\beta} \end{bmatrix} \begin{bmatrix} 0 & 0 & 0 \\ -\mathrm{c}_\alpha \mathrm{t}_\beta & 1 & -\mathrm{s}_\alpha \mathrm{t}_\beta \\ \mathrm{s}_\alpha & 0 & -\mathrm{c}_\alpha \end{bmatrix} \begin{bmatrix} p \\ q \\ r \end{bmatrix} + g \begin{bmatrix} 0 & -\mathrm{c}_\phi \mathrm{c}_\theta & \mathrm{s}_\phi \mathrm{c}_\theta \\ \mathrm{c}_\phi \mathrm{c}_\theta & 0 & \mathrm{s}_\theta \\ -\mathrm{s}_\phi \mathrm{c}_\theta & -\mathrm{s}_\theta & 0 \end{bmatrix} \begin{bmatrix} p \\ q \\ r \end{bmatrix} \\ &+ \tfrac{1}{m}\bar{q}S \begin{bmatrix} C_{X_{\delta_a}} & C_{X_{\delta_e}} & C_{X_{\delta_r}} \\ C_{Y_{\delta_a}} & C_{Y_{\delta_e}} & C_{Y_{\delta_r}} \\ C_{Z_{\delta_a}} & C_{Z_{\delta_e}} & C_{Z_{\delta_r}} \end{bmatrix} \begin{bmatrix} \dot{\delta}_a \\ \dot{\delta}_e \\ \dot{\delta}_r \end{bmatrix}. \end{aligned}$$

Therefore, expanding these equations, substituting the aerodynamic force coefficients from (20)-(21), taking partial derivatives of (20)-(21) to obtain aerodynamic derivatives of force coefficients (that is, $C_{X_\alpha} = \partial C_X/\partial\alpha$, etc.), and noting that $C_{Y_{\delta_a}} = C_{Y_{\delta_r}} = C_{Z_{\delta_a}} = C_{Z_{\delta_r}} = 0$, algebraic manipulations yield the following nonlinear representations of missile body acceleration dynamics:

$$\left.\begin{aligned} \dot{a}_{X_B} &= (X_{a_X} a_{X_B} + X_{a_Y} a_{Y_B} + X_{a_Z} a_{Z_B})M + X_{M^2} M^2 + X_p p + X_q q + X_r r \\ \dot{a}_{Y_B} &= (Y_{a_X} a_{X_B} + Y_{a_Y} a_{Y_B} + Y_{a_Z} a_{Z_B})M + Y_{M^2} M^2 + Y_p p + Y_q q + Y_r r \\ \dot{a}_{Z_B} &= (Z_{a_X} a_{X_B} + Z_{a_Y} a_{Y_B} + Z_{a_Z} a_{Z_B})M + Z_{M^2} M^2 + Z_p p + Z_q q + Z_r r, \end{aligned}\right\} \quad (32)$$

where

$$\begin{aligned} C_{X_\alpha} &= 2a_1\alpha + a_3\delta_e & C_{Y_\alpha} &\approx 2b_3\alpha\beta + \tfrac{d}{2V} C_{Y_{pa}} p & C_{Z_\alpha} &\approx c_1 + 2c_2\alpha + c_3|\alpha| + 3c_4\alpha^2 + c_5\beta^2 \\ C_{X_\beta} &= 2a_2\beta + a_4\delta_r & C_{Y_\beta} &\approx b_1 + 2b_2\beta + b_3|\beta| + 3b_4\beta^2 + b_5\alpha^2 & C_{Z_\beta} &\approx 2c_5\alpha\beta + \tfrac{d}{2V} C_{Y_{pa}} p \\ C_{X_{\delta_e}} &= 2a_7\delta_a & C_{X_{\delta_a}} &= a_3\alpha + 2a_5\delta_e & C_{X_{\delta_r}} &= a_4\beta + 2a_6\delta_r \end{aligned}$$

$$\begin{aligned} X_{a_X} &\triangleq \lambda(2C'_{X_j}\,\mathrm{c}_\alpha \mathrm{c}_\beta - C_{X_\alpha}\,\mathrm{s}_\alpha/\mathrm{c}_\beta - C_{X_\beta}\,\mathrm{c}_\alpha \mathrm{s}_\beta) & X_p &\triangleq \lambda M^2 a(-C_{X_\alpha}\,\mathrm{c}_\alpha \mathrm{t}_\beta + C_{X_\beta}\,\mathrm{s}_\alpha) \\ X_{a_Y} &\triangleq \lambda(2C'_{X_j}\,\mathrm{s}_\beta + C_{X_\beta}\,\mathrm{c}_\beta) & X_q &\triangleq \lambda M^2 a C_{X_\alpha} - g\,\mathrm{c}_\phi \mathrm{c}_\theta \\ X_{a_Z} &\triangleq \lambda(2C'_{X_j}\,\mathrm{s}_\alpha \mathrm{c}_\beta + C_{X_\alpha}\,\mathrm{c}_\alpha/\mathrm{c}_\beta - C_{X_\beta}\,\mathrm{s}_\alpha \mathrm{s}_\beta) & X_r &\triangleq -\lambda M^2 a(C_{X_\alpha}\,\mathrm{s}_\alpha \mathrm{t}_\beta + C_{X_\beta}\,\mathrm{c}_\alpha) + g\,\mathrm{s}_\phi \mathrm{c}_\theta \\ X_{M^2} &\triangleq \lambda a(C_{X_{\delta_a}}\dot{\delta}_a + C_{X_{\delta_e}}\dot{\delta}_e + C_{X_{\delta_r}}\dot{\delta}_r) \end{aligned}$$

$$\begin{aligned} Y' &\triangleq 2C'_Y - \tfrac{d}{(Ma)^2} C_{Y_\beta}(a_{X_B}\,\mathrm{c}_\alpha \mathrm{s}_\beta - a_{Y_B}\,\mathrm{c}_\beta + a_{Z_B}\,\mathrm{s}_\alpha \mathrm{s}_\beta) & Z' &\triangleq 2C'_Z + \tfrac{d}{(Ma)^2} C_{Z_\alpha}(a_{Z_B}\,\mathrm{c}_\alpha - a_{X_B}\,\mathrm{s}_\alpha) \\ Y_{a_X} &\triangleq \lambda(Y'\,\mathrm{c}_\alpha \mathrm{c}_\beta - C_{Y_\alpha}\,\mathrm{s}_\alpha/\mathrm{c}_\beta - C_{Y_\beta}\,\mathrm{c}_\alpha \mathrm{s}_\beta) & Z_{a_X} &\triangleq \lambda(Z'\,\mathrm{c}_\alpha \mathrm{c}_\beta - C_{Z_\alpha}\,\mathrm{s}_\alpha/\mathrm{c}_\beta - C_{Z_\beta}\,\mathrm{c}_\alpha \mathrm{s}_\beta) \\ Y_{a_Y} &\triangleq \lambda(Y'\,\mathrm{s}_\beta + C_{Y_\beta}\,\mathrm{c}_\beta) & Z_{a_Y} &\triangleq \lambda(Z'\,\mathrm{s}_\beta + C_{Z_\beta}\,\mathrm{c}_\beta) \\ Y_{a_Z} &\triangleq \lambda(Y'\,\mathrm{s}_\alpha \mathrm{c}_\beta + C_{Y_\alpha}\,\mathrm{c}_\alpha/\mathrm{c}_\beta - C_{Y_\beta}\,\mathrm{s}_\alpha \mathrm{s}_\beta) & Z_{a_Z} &\triangleq \lambda(Z'\,\mathrm{s}_\alpha \mathrm{c}_\beta + C_{Z_\alpha}\,\mathrm{c}_\alpha/\mathrm{c}_\beta - C_{Z_\beta}\,\mathrm{s}_\alpha \mathrm{s}_\beta) \\ Y_{M^2} &\triangleq \lambda a C_{Y_{\delta_r}}\dot{\delta}_r & Z_{M^2} &\triangleq \lambda a C_{Z_{\delta_e}}\dot{\delta}_e \\ Y_p &\triangleq \lambda M^2 a(-C_{Y_\alpha}\,\mathrm{c}_\alpha \mathrm{t}_\beta + C_{Y_\beta}\,\mathrm{s}_\alpha) & Z_p &\triangleq \lambda M^2 a(-C_{Z_\alpha}\,\mathrm{c}_\alpha \mathrm{t}_\beta + C_{Z_\beta}\,\mathrm{s}_\alpha) \\ &\quad + \lambda\dot{M}d(C_{Y_{pa}}\alpha + C_{Y_\beta}\,\mathrm{s}_\alpha) + g\,\mathrm{c}_\phi \mathrm{c}_\theta & &\quad + \lambda\dot{M}d(C_{Y_{pa}}\beta - C_{Z_\alpha}\,\mathrm{c}_\alpha \mathrm{t}_\beta) - g\,\mathrm{s}_\phi \mathrm{c}_\theta \\ Y_q &\triangleq \lambda M^2 a C_{Y_\alpha} & Z_q &\triangleq \lambda M^2 a C_{Z_\alpha} + \lambda\dot{M}d(C_{Z_q} + C_{Z_{\dot\alpha}}) - g\,\mathrm{s}_\theta \\ Y_r &\triangleq -\lambda M^2 a(C_{Y_\alpha}\,\mathrm{s}_\alpha \mathrm{t}_\beta + C_{Y_\beta}\,\mathrm{c}_\alpha) & Z_r &\triangleq -\lambda M^2 a(C_{Z_\alpha}\,\mathrm{s}_\alpha \mathrm{t}_\beta + C_{Z_\beta}\,\mathrm{c}_\alpha) \\ &\quad + \lambda\dot{M}d(C_{Y_q} - C_{Y_{\dot\beta}}\,\mathrm{c}_\alpha) + g\,\mathrm{s}_\theta & &\quad - \lambda\dot{M}d C_{Z_{\dot\alpha}}\,\mathrm{s}_\alpha \mathrm{t}_\beta \end{aligned}$$

with $\lambda \triangleq \frac{1}{2m}\rho a S$. Here C'_X, C'_Y, C'_Z are obtained directly from (21), whereas C_X and $\dot{M}$ from (20) and (25), respectively.

3.7 Bank Angle Dynamics

The respective angular velocities $\boldsymbol{\omega}_{W/E}$ and $\boldsymbol{\omega}_{B/E}$ of the wind frame $\mathcal{F}_W$ and the body frame $\mathcal{F}_B$ w.r.t. the Earth frame $\mathcal{F}_E$ are related by

$$\boldsymbol{\omega}_{B/E} = \boldsymbol{\omega}_{W/E} - \dot{\beta}\mathbf{k}_W + \dot{\alpha}\mathbf{j}_B.$$

Resolving this equation in body coordinates gives

$$\boldsymbol{\omega}_{B/E}^{(B)} = \mathbf{T}^{(B,W)}\boldsymbol{\omega}_{W/E}^{(W)} - \dot{\beta}\mathbf{T}^{(B,W)}\mathbf{k}_W + \dot{\alpha}\mathbf{j}_B,$$

so that $\boldsymbol{\omega}_{W/E}^{(W)}$ can be expressed in component form as

$$\boldsymbol{\omega}_{W/E}^{(W)} = \mathbf{T}^{(W,B)}[p - \dot{\beta}\,\mathrm{s}_\alpha \quad q - \dot{\alpha} \quad r + \dot{\beta}c_\alpha]^T, \quad (33)$$

with $\mathbf{T}^{(W,B)}$ obtained from (2). A relationship between the angular rates $\dot{\mu}, \dot{\gamma}, \dot{\chi}$ and the wind-fixed angular rates $\boldsymbol{\omega}_{W/E}^{(W)}$ can also be derived using a χ-γ-μ sequence of rotations from fixed-Earth coordinates to wind coordinates, giving

$$\boldsymbol{\omega}_{W/E}^{(W)} = \begin{bmatrix} 1 & 0 & -\mathrm{s}_\gamma \\ 0 & \mathrm{c}_\mu & \mathrm{s}_\mu \mathrm{c}_\gamma \\ 0 & -\mathrm{s}_\mu & \mathrm{c}_\mu \mathrm{c}_\gamma \end{bmatrix} \begin{bmatrix} \dot{\mu} \\ \dot{\gamma} \\ \dot{\chi} \end{bmatrix}.$$

Inverting this matrix equation and substituting into (33) gives

$$\begin{bmatrix} \dot{\mu} \\ \dot{\gamma} \\ \dot{\chi} \end{bmatrix} = \begin{bmatrix} 1 & \mathrm{t}_\gamma \mathrm{s}_\mu & \mathrm{t}_\gamma \mathrm{c}_\mu \\ 0 & \mathrm{c}_\mu & -\mathrm{s}_\mu \\ 0 & \mathrm{s}_\mu/\mathrm{c}_\gamma & \mathrm{c}_\mu/\mathrm{c}_\gamma \end{bmatrix} \begin{bmatrix} \mathrm{c}_\alpha \mathrm{c}_\beta & \mathrm{s}_\beta & \mathrm{s}_\alpha \mathrm{c}_\beta \\ -\mathrm{c}_\alpha \mathrm{s}_\beta & \mathrm{c}_\beta & -\mathrm{s}_\alpha \mathrm{s}_\beta \\ -\mathrm{s}_\alpha & 0 & \mathrm{c}_\alpha \end{bmatrix} \begin{bmatrix} p - \dot{\beta}\,\mathrm{s}_\alpha \\ q - \dot{\alpha} \\ r + \dot{\beta}c_\alpha \end{bmatrix}.$$

The required equation for $\dot{\mu}$ is then obtained from the above relation by expanding it and substituting (26) and (27) for $\dot{\alpha}$ and $\dot{\beta}$, respectively, thus obtaining the bank angle dynamics

$$\begin{aligned} \dot{\mu} = p\tfrac{\mathrm{c}_\alpha}{\mathrm{c}_\beta} + r\tfrac{\mathrm{s}_\alpha}{\mathrm{c}_\beta} + \tfrac{1}{Ma}[&a_{X_B}(\mathrm{s}_\alpha \mathrm{t}_\beta + \mathrm{s}_\alpha \mathrm{t}_\gamma \mathrm{s}_\mu - \mathrm{c}_\alpha \mathrm{s}_\beta \mathrm{t}_\gamma \mathrm{c}_\mu) \\ &+ a_{Y_B}(\mathrm{c}_\beta \mathrm{t}_\gamma \mathrm{c}_\mu) - a_{Z_B}(\mathrm{s}_\alpha \mathrm{s}_\beta \mathrm{t}_\gamma \mathrm{c}_\mu + \mathrm{c}_\alpha \mathrm{t}_\beta + \mathrm{c}_\alpha \mathrm{t}_\gamma \mathrm{s}_\mu)]. \end{aligned} \quad (34)$$

3.8 Flight Path Angle Dynamics

For a flat Earth,

$$d_E\mathbf{V}/dt = d_V\mathbf{V}/dt + \boldsymbol{\omega}_{V/E} \times \mathbf{V} = \mathbf{F}/m(t),$$

which can be expressed in velocity coordinates as

$$d_V\mathbf{V}^{(V)}/dt + \boldsymbol{\omega}_{V/E}^{(V)} \times \mathbf{V}^{(V)} = \mathbf{F}^{(V)}/m, \quad (35)$$

where $\mathbf{V}^{(V)} = [V \quad 0 \quad 0]^T$ and thus $d_V\mathbf{V}^{(V)}/dt = [\dot{V} \quad 0 \quad 0]^T$. The angular velocity $\boldsymbol{\omega}_{V/E}$ of the velocity frame $\mathcal{F}_V$ w.r.t. the Earth frame $\mathcal{F}_E$ consists of the vector addition of the flight path angular rates $\dot{\chi}$ and $\dot{\gamma}$ times their respective unit vectors so that, by resolving $\boldsymbol{\omega}_{V/E}$ in velocity coordinates, the following coordinated equation is obtained for expressing the velocity-fixed angular rates $\boldsymbol{\omega}_{V/E}^{(V)}$ in component form:

$$\boldsymbol{\omega}_{V/E}^{(V)} = \dot{\gamma}\begin{bmatrix} 0 \\ 1 \\ 0 \end{bmatrix} + \dot{\chi}\begin{bmatrix} \mathrm{c}_\gamma & 0 & -\mathrm{s}_\gamma \\ 0 & 1 & 0 \\ \mathrm{s}_\gamma & 0 & \mathrm{c}_\gamma \end{bmatrix}\begin{bmatrix} 0 \\ 0 \\ 1 \end{bmatrix} = \begin{bmatrix} -\dot{\chi}\,\mathrm{s}_\gamma \\ \dot{\gamma} \\ \dot{\chi}\,\mathrm{c}_\gamma \end{bmatrix}.$$

Now, since $\mathbf{F}^{(V)} = \mathbf{F}_g^{(V)} + \mathbf{F}_a^{(V)} + \mathbf{F}_p^{(V)}$,

$$\mathbf{F}^{(V)} = m\mathbf{T}^{(V,E)}\mathbf{g}^{(E)} + \mathbf{T}^{(V,W)}\mathbf{T}^{(W,B)}[\mathbf{F}_a^{(B)} + \mathbf{F}_p^{(B)}].$$

Noting that $\mathbf{F}_a^{(B)} + \mathbf{F}_p^{(B)} = m[\mathbf{a}^{(B)} - \mathbf{g}^{(B)}]$ yields

$$\mathbf{F}^{(V)}/m = \mathbf{T}^{(V,E)}\mathbf{g}^{(E)} + \mathbf{T}^{(V,W)}\mathbf{T}^{(W,B)}[\mathbf{a}^{(B)} - \mathbf{g}^{(B)}],$$

which is now conveniently expressed in terms of the body accelerations $\mathbf{a}^{(B)}$. Substituting these expressions for $\boldsymbol{\omega}_{V/E}^{(V)}$ and $\mathbf{F}^{(V)}/m$ into (35) with (22) for V, using the coordinate transformation matrices derived in Section 2.2, and solving for $\dot{\gamma}$ and $\dot{\chi}$, the expressions for flight path angle dynamics are obtained as

$$\left.\begin{aligned}\dot{\gamma} &= \tfrac{1}{Ma}[(\mathrm{s}_\alpha \mathrm{c}_\mu + \mathrm{c}_\alpha \mathrm{s}_\beta \mathrm{s}_\mu)a_{X_B} - \mathrm{c}_\beta \mathrm{s}_\mu a_{Y_B} - (\mathrm{c}_\alpha \mathrm{c}_\mu - s_\alpha s_\beta \mathrm{s}_\mu)a_{Z_B} + g_1] \\ \dot{\chi} &= \tfrac{1}{Ma\mathrm{c}_\gamma}[(\mathrm{s}_\alpha \mathrm{s}_\mu - \mathrm{c}_\alpha \mathrm{s}_\beta \mathrm{c}_\mu)a_{X_B} + \mathrm{c}_\beta \mathrm{c}_\mu a_{Y_B} - (\mathrm{c}_\alpha \mathrm{s}_\mu + s_\alpha \mathrm{s}_\beta \mathrm{c}_\mu)a_{Z_B} + g_2],\end{aligned}\right\} \quad (36)$$

where

$$g_1 \triangleq g[(\mathrm{c}_\alpha \mathrm{s}_\beta \mathrm{s}_\theta + \mathrm{c}_\beta \mathrm{s}_\phi \mathrm{c}_\theta - s_\alpha s_\beta \mathrm{c}_\phi \mathrm{c}_\theta)\mathrm{s}_\mu + (\mathrm{s}_\alpha \mathrm{s}_\theta + \mathrm{c}_\alpha \mathrm{c}_\phi \mathrm{c}_\theta)\mathrm{c}_\mu - \mathrm{c}_\gamma]$$
$$g_2 \triangleq -g[(\mathrm{c}_\alpha \mathrm{s}_\beta \mathrm{s}_\theta + \mathrm{c}_\beta \mathrm{s}_\phi \mathrm{c}_\theta - s_\alpha \mathrm{s}_\beta \mathrm{c}_\phi \mathrm{c}_\theta)\mathrm{c}_\mu + (\mathrm{s}_\alpha \mathrm{s}_\theta + \mathrm{c}_\alpha \mathrm{c}_\phi \mathrm{c}_\theta)\mathrm{s}_\mu].$$

3.9 Altitude Dynamics

Transforming the components of $\mathbf{V}^{(V)}$ to the fixed-Earth coordinate system gives

$$\mathbf{V}^{(E)} = \mathbf{T}^{(E,V)}\mathbf{V}^{(V)} = V[\mathrm{c}_\gamma \mathrm{c}_\chi \quad \mathrm{c}_\gamma \mathrm{s}_\chi \quad -\mathrm{s}_\gamma]^T.$$

Thus the dynamics for the altitude h is obtained from the negative Z_E component of $\mathbf{V}^{(E)}$, so that using (22) gives

$$\dot{h} = Ma\,\mathrm{s}_\gamma. \quad (37)$$

4. AUTOPILOT STRUCTURE

All equations are now in place to proceed with nonlinear autopilot development, which is based on the dynamic models derived in Section 3. Note that these dynamic models are very general compared to all other nonlinear approaches proposed in the literature for missile autopilot design.

4.1 Autopilot Design Models

Maximizing overall missile performance requires choosing the appropriate autopilot command structure for each mission phase. This may include designing different autopilots for launch, an agile turn at high angle of attack, midcourse where a long flyout is required, and endgame where terminal homing maneuvers are necessary. The missile autopilot can command *accelerations*, *body rates*, *incidence angles*, and *flight path angles*. For example, vertical launch surface-air missiles may require flight path angle commands during the launch phase. For air-air missiles, on the other hand, a body rate command is typically used during launch, since rate-command autopilots are very robust to the uncertain proximity aerodynamics (Wise & Broy, 1998). An agile turn requires directional control of the missile's velocity vector relative to the missile body (given by incidence angles). This necessitates following angle-of-attack and sideslip angle commands, and regulating roll to zero. Finally, during midcourse and terminal phases, an acceleration autopilot is generally used. Some missiles, such as cruise missiles, also employ altitude-hold autopilots.

In what follows, a generic approach for nonlinear missile autopilot design will be developed using the complete set of nonlinear dynamic equations (20)-(37) derived in Section 3 for missile flight control systems. In the development of this generic approach, the proposed topology will accommodate all the abovementioned autopilot structures.

4.2 Autopilot Design Topology

In flight dynamics, *short-period mode* is primarily described by body rates and incidence angles, whereas *long-period* (*phugoid*) *mode* is primarily described by flight path angles. In addition to this two-layer structure that exists between short-period and long-period modes, flight vehicles also experience inherent time-scale separation between "*slow*" *translational dynamics* and "*fast*" *rotational dynamics* of the short-period mode. This phenomenon causes autopilot design philosophies based on a single unified (single loop) framework to be ineffective, because control surface deflections directly respond to the translational error correction demands, which may lead to instability of the rotational dynamics. This is especially true for control surfaces located either at the front or the tail of the missile, because deflections of these control surfaces can create only minor forces, whereas they create large moments due to a long moment arm from the CM. Consequently, these control surfaces are ineffective in directly correcting translational errors, whereas they can be very effective in turning the flight vehicle. Therefore, for a successful flight control system, the design must exploit the time-scale separation that exists between translational and rotational motions of the CM.

In the development of the generic approach to missile autopilot design in this study, the proposed structure explicitly exploits the inherent time-scale separation that exists between translational and rotational motions of flight vehicles, as well as between short-period and long-period motions. The former issue is addressed using a two-loop autopilot design topology, as opposed to using a single-loop structure. The latter issue is addressed by an additional outer loop, giving the three-loop structure presented in Fig. 5. The outer loop converts flight path angle commands (γ^{com}, χ^{com}) or altitude commands (h^{com}) from the guidance system to bank angle commands, together with either incidence angle commands ($\alpha^{com}, \beta^{com}$) or lateral-normal (pitch and yaw) body acceleration commands ($a_{Y_B}^{com}, a_{Y_B}^{com}$) for the intermediate loop. The intermediate loop then converts these incidence angles or body accelerations to body roll rate, pitch rate and yaw rate commands ($p^{com}, q^{com}, r^{com}$) for the inner loop. Finally, the inner loop converts $p^{com}, q^{com}, r^{com}$ to actual control surface deflection commands δ_i^{com} ($i = 1, \ldots, 4$) for the actuators.

In the design, full nonlinear and coupled 6-DOF equations of motion describing missile dynamics derived in Section 3 are directly used in all three loops, without making any simplifications to these equations. This is achieved by formulating the equations in *state-dependent nonlinear form* for each loop for controller design, which is discussed next.

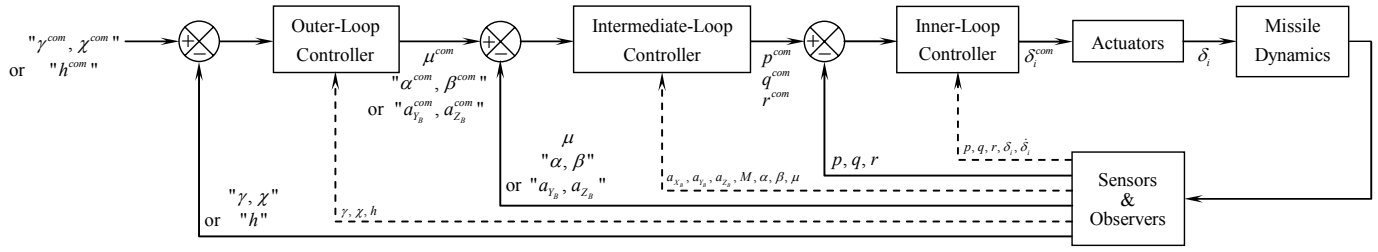

Fig. 5. Three-Loop Autopilot Design Topology

5. STATE-DEPENDENT NONLINEAR FORMULATION

The first objective is to represent the equations for each loop in Fig. 5 in the input-affine form

$$\dot{\mathbf{x}}(t) = \mathbf{f}(\mathbf{x}) + \mathbf{B}(\mathbf{x})\mathbf{u}(t), \quad \mathbf{x}(0) = \mathbf{x}_0 \tag{38}$$

with state vector $\mathbf{x} \in \mathbb{R}^n$ and (unconstrained) input vector $\mathbf{u} \in \mathbb{R}^m$, where $\mathbf{f}(\mathbf{x})$ is a continuously differentiable vector-valued function of $\mathbf{x}$, that is, $\mathbf{f}(\cdot) \in C^1$, and the origin $\mathbf{x} = \mathbf{0}$ is an *equilibrium point* of the system with $\mathbf{u} = \mathbf{0}$, such that $\mathbf{f}(\mathbf{0}) = \mathbf{0}$, and $\mathbf{B}(\mathbf{x}) \neq \mathbf{0} \ \ \forall \mathbf{x}$. Readers may refer to Çimen (2010) for an overview of the various methods available for systematically handling numerous systems that do not meet the basic structure and conditions mentioned above. Once the systems meet the proper structure and conditions, the concept of *extended linearization* is used to formulate the nonlinear vehicle dynamics in SDC form (Çimen, 2010). Thus, the input-affine nonlinear system (38) is represented in the form

$$\dot{\mathbf{x}}(t) = \mathbf{A}(\mathbf{x})\mathbf{x}(t) + \mathbf{B}(\mathbf{x})\mathbf{u}(t), \quad \mathbf{x}(0) = \mathbf{x}_0, \tag{39}$$

which has a linear structure with SDC matrices $\mathbf{A}(\mathbf{x})$ and $\mathbf{B}(\mathbf{x})$. Note that in a deterministic setting, the SDC parameterization (39) fully captures the nonlinearities of the system. Although the SDC parameterization is *unique* in the case of *scalar* x for all x, it is *nonunique* in the *multivariable* case, and the SDC parameterization $\mathbf{A}(\mathbf{x})$ itself can be parameterized as $\mathbf{A}(\mathbf{x}, \boldsymbol{\sigma})$, where $\boldsymbol{\sigma}$ is a vector of free design parameters (see Proposition 1 in Çimen, 2010). The introduction of $\boldsymbol{\sigma}$ creates additional degrees of freedom that can be used to enhance controller performance, avoid singularities or loss of controllability, and affect tradeoffs between optimality, stability, robustness, and disturbance rejection, thus offering a very flexible nonlinear control policy.

The primary condition in selecting the "right" $\mathbf{A}(\mathbf{x})$ is that the respective pairs $\{\mathbf{A}(\mathbf{x}), \mathbf{B}(\mathbf{x})\}$ are *pointwise stabilizable* SDC parameterizations of the nonlinear system (38) $\forall \mathbf{x} \in \Omega$. In addition to satisfying this requirement, a *rule of thumb* in selecting the state-dependent factorization is that any term containing more than one state variable must be parameterized and apportioned among the corresponding elements of the $\mathbf{A}(\mathbf{x}, \boldsymbol{\sigma})$ matrix (Cloutier & Stansbery, 2002b). For example, if $\dot{x}_3 = x_1 x_2$, $\mathbf{A}(\mathbf{x}) = [a_{ij}]$ is parameterized with $a_{31} = \sigma_1 x_2$ and $a_{32} = (1 - \sigma_1) x_1$. The free design parameter σ_1 can be selected to have *any finite real value*, but is *generally chosen* in the range [0,1]. It is also desirable to shift state-dependent factors which exclude the origin even though they are embedded in a term which goes to zero as the state goes to zero, as discussed in Cloutier & Stansbery (2002a,b) and Çimen (2010). For example, consider $\dot{x}_2 = x_3 \cos x_1$. Obviously, this term goes to zero as x_3 goes to zero, but it is desirable to have a nonzero entry in the (2,1)-element of the $\mathbf{A}(\mathbf{x}, \boldsymbol{\sigma})$ matrix that reflects the fact that $\dot{x}_2$ depends on x_1. This is accomplished by shifting the term so that it goes through the origin. For the given example, adding and subtracting 1 gives $\cos x_1 = [\cos x_1 - 1] + 1$. The function $\cos x_1 - 1$ goes through the origin and can therefore be factored as $\cos x_1 - 1 = [(\cos x_1 - 1)/x_1] x_1$. Note that the expression in brackets is well-behaved at the origin, when $x_1 = 0$. Then, by writing $\dot{x}_2 = [(\cos x_1 - 1)/x_1] x_1 x_3 + x_3$ allows the system to be parameterized as $a_{21} = \sigma_2 [(\cos x_1 - 1)/x_1] x_3$ and $a_{23} = (1 - \sigma_2)(\cos x_1 - 1) + 1$, which yields the desired nonzero entry in a_{21}. Such an approach provides a complete characterization of the possible factorizations of $\mathbf{f}(\mathbf{x})$ into $\mathbf{A}(\mathbf{x}, \boldsymbol{\sigma})\mathbf{x}$, where $\boldsymbol{\sigma} = [\sigma_1, \ldots, \sigma_k]$.

5.1 State-Dependent Formulation of the Inner Loop

Consider the body-rate dynamics derived in (31), and note the presence of the state-independent terms (referred to as *bias* terms) L_{bias}, M_{bias}, N_{bias}, which prevents a direct C^1 factorization of $\mathbf{f}(\mathbf{x})$ into $\mathbf{A}(\mathbf{x}, \boldsymbol{\alpha})\mathbf{x}$ for SDC representation of (31). In general, within the framework of state-dependent parameterization, bias terms are handled by multiplying and dividing these terms by a state that will never go to zero (Cloutier & Stansbery, 2001; Çimen, 2010). However, the three states p, q, r can all go to zero. Alternatively, if the bias term is constant or slowly-varying, then it can be modeled as a stable state $\dot{b}(t) = -\lambda b(t)$, where λ is a small positive number. Each time through the controller, the *actual value* of $b(t)$ would then be used in calculating the control $\mathbf{u}$. However, L_{bias}, M_{bias} and N_{bias} are neither constant nor slowly-varying due to their dependence on $M, \alpha, \beta, \dot{\alpha}, \dot{\beta}$ and $\bar{q}$. A third alternative is to introduce an additional state s with stable dynamics $\dot{s}(t) = -\lambda_s s(t)$, $\lambda_s > 0$, for the purpose of absorbing the biases. Augmenting the system with the stable state, bias terms can then be factored as $b = [b/s]s$, where b denotes the biases $L_{bias}, M_{bias}, N_{bias}$. Each time through the inner-loop controller, the *initial value* $s(0)$ (assumed small) is used in the SDC matrix in calculating $\mathbf{u}$.

Thus, defining the state vector $\mathbf{x} \triangleq [p \quad q \quad r \quad s]^T$ and control vector $\mathbf{u} \triangleq [\delta_a \quad \delta_e \quad \delta_r]^T$, (31) can now be represented (nonuniquely) in SDC form (39). Following the systematic procedure described above, any term containing more than one state variable must first be parameterized and then apportioned among the corresponding elements of the $\mathbf{A}$ matrix. There are five such terms in (31), each containing a pair of state variables. Thus, introducing the vector $\boldsymbol{\sigma}_1$ with five design parameters $\sigma_{1,1}, \ldots, \sigma_{1,5} \in \mathbb{R}$, these terms can all be parameterized, and a family of SDC parameterizations for the system can then be constructed with

$$\mathbf{A}(\mathbf{x}, \boldsymbol{\sigma}_1) = \begin{bmatrix} a_{11} & a_{12} & a_{13} & \frac{1}{s}L_{bias} \\ a_{21} & a_{22} & a_{23} & \frac{1}{s}M_{bias} \\ a_{31} & a_{32} & a_{33} & \frac{1}{s}N_{bias} \\ 0 & 0 & 0 & -\lambda_s \end{bmatrix}, \ \mathbf{B} = \begin{bmatrix} L_{\delta_a} & L_{\delta_e} & L_{\delta_r} \\ 0 & M_{\delta_e} & 0 \\ N_{\delta_a} & N_{\delta_e} & N_{\delta_r} \\ 0 & 0 & 0 \end{bmatrix}, \tag{40}$$

where the a_{ij} elements of the inner-loop SDC matrix $\mathbf{A}(\mathbf{x}, \boldsymbol{\sigma}_1)$ are presented in Appendix A.1. State-dependent nonlinear formulation of the inner loop is then based on the complete set of dynamic equations (28), (30) and (40). Therefore, for control design, the inner loop is represented in SDC form by the augmented system

$$\dot{\mathbf{x}}_{IL} = \mathbf{A}_{IL}(\mathbf{x}_{IL})\mathbf{x}_{IL} + \mathbf{B}_{IL}\mathbf{u}_{IL} \tag{41}$$

with the respective state and control input vectors

$$\mathbf{x}_{IL} \triangleq [\mathbf{x}^T \quad \boldsymbol{\delta}^T \quad \dot{\boldsymbol{\delta}}^T]^T, \quad \mathbf{u}_{IL} \triangleq \boldsymbol{\delta}^{com}.$$

Using the relationship $\mathbf{u} = \boldsymbol{\Delta}_{\text{logic}}\boldsymbol{\delta}$ from (28), together with (30) yields the SDC matrices for the inner loop as

$$\mathbf{A}_{IL}(\mathbf{x}_{IL}) \triangleq \begin{bmatrix} \mathbf{A}(\mathbf{x}, \boldsymbol{\sigma}_1) & \mathbf{B}\boldsymbol{\Delta}_{\text{logic}} & \mathbf{0}_{4\times4} \\ \mathbf{0}_{4\times4} & \mathbf{0}_{4\times4} & \mathbf{I}_{4\times4} \\ \mathbf{0}_{4\times4} & -\omega_n^2 \operatorname{diag}\left\{\frac{\operatorname{sat}(\delta_i, \delta_{i\max})}{\delta_i}\right\} & -2\zeta\omega_n^2 \operatorname{diag}\left\{\frac{\operatorname{sat}(\dot{\delta}_i, \dot{\delta}_{i\max})}{\dot{\delta}_i}\right\} \end{bmatrix}, \mathbf{B}_{IL} \triangleq \begin{bmatrix} \mathbf{0}_{8\times4} \\ \omega_n^2 \mathbf{I}_{4\times4} \end{bmatrix} \tag{42}$$

for $i = 1, \ldots, 4$, with $\mathbf{A}(\mathbf{x}, \boldsymbol{\sigma}_1)$ and $\mathbf{B}$ constructed as in (40).

State-dependent nonlinear formulation of the inner-loop given by (41) and (42) incorporates hard bounds on the control surface deflection angles δ_i and their rates $\dot{\delta}_i$. This is accomplished using the second-order nonlinear actuator dynamics given by (30). This is different from the inner-loop

design of the missile control problem presented by Cloutier & Stansbery (2001), where zero-order (that is, lag-free) actuator dynamics was assumed with hard bounds imposed only on the effective control surface deflections angles ($\delta_a, \delta_e, \delta_r$) using integral control. In reality, however, these constraints take effect on individual control surfaces δ_i ($i = 1, \ldots, 4$), which makes the approach proposed here more practical. Note also that without actuator dynamics, imposing hard bounds on both δ_i and $\dot{\delta}_i$ would require the use of double integral control.

5.2 State-Dependent Formulation of the Intermediate Loop

For state-dependent nonlinear formulation of the intermediate loop, let us define the state vector and the control vector as

$$\mathbf{x}_{ML} \triangleq [a_{X_B} \quad a_{Y_B} \quad a_{Z_B} \quad M \quad \alpha \quad \beta \quad \mu]^T, \ \mathbf{u}_{ML} \triangleq [p \quad q \quad r]^T.$$

Since p, q, r are the controls in the intermediate loop, the *current values* of the control surface deflections δ_j and their rates $\dot{\delta}_j$ ($j = a, e, r$) are used in this loop.

Since thrust is not controllable, the controllability of the Mach dynamics (25) is due to angle of attack and sideslip angle. Consequently, Mach controllability is lost when α and β are both zero, as also noted by Cloutier & Stansbery (2001). Therefore, similar to Cloutier & Stansbery (2001), a stabilizing term of $-0.1M$ is added to the Mach dynamics so as to eliminate loss of controllability in the state-dependent formulation of the intermediate-loop dynamics (Çimen, 2010).

Eqs. (25), (26), (27), (32) and (34) can now be represented in SDC form (39). Once again, following the systematic procedure previously described, any term containing more than one state variable must first be parameterized and then apportioned among the corresponding elements of the $\mathbf{A}$ matrix. Note that multiples of three individual states, say $\dot{x}_1 = x_1 x_2 x_3$, can be parameterized as $a_{11} = \frac{1}{3}(\sigma_1 + \sigma_2) x_2 x_3$, $a_{12} = \frac{1}{3}(1 - \sigma_1 + \sigma_3) x_1 x_3$, $a_{13} = \frac{1}{3}(2 - \sigma_2 - \sigma_3) x_1 x_2$. Therefore, a vector $\boldsymbol{\sigma}_2$ with 42 design parameters $\sigma_{2,1}, \sigma_{2,2}, \ldots, \sigma_{2,42} \in \mathbb{R}$ is introduced, which is used in parameterizing nonlinear terms in these equations. A hypersurface of SDC parameterizations for the intermediate-loop system is then constructed with

$$\mathbf{A}_{ML}(\mathbf{x}_{ML}, \boldsymbol{\sigma}_2) = \begin{bmatrix} a_{11} & a_{12} & a_{13} & a_{14} & 0 & 0 & 0 \\ a_{21} & a_{22} & a_{23} & a_{24} & 0 & 0 & 0 \\ a_{31} & a_{32} & a_{33} & a_{34} & 0 & 0 & 0 \\ a_{41} & a_{42} & a_{43} & -0.1 & a_{45} & a_{46} & 0 \\ a_{51} & 0 & a_{53} & 0 & a_{55} & 0 & 0 \\ a_{61} & a_{62} & a_{63} & 0 & a_{65} & a_{66} & 0 \\ a_{71} & a_{72} & a_{73} & 0 & a_{75} & a_{76} & a_{77} \end{bmatrix}, \mathbf{B}_{ML}(\mathbf{x}_{ML}) = \begin{bmatrix} X_p & X_q & X_r \\ Y_p & Y_q & Y_r \\ Z_p & Z_q & Z_r \\ 0 & 0 & 0 \\ -\mathrm{c}_\alpha \mathrm{t}_\beta & 1 & -\mathrm{s}_\alpha \mathrm{t}_\beta \\ \mathrm{s}_\alpha & 0 & -\mathrm{c}_\alpha \\ \mathrm{c}_\alpha / \mathrm{c}_\beta & 0 & \mathrm{s}_\alpha / \mathrm{c}_\beta \end{bmatrix}, \quad (43)$$

where the a_{ij} elements of the intermediate-loop SDC matrix $\mathbf{A}_{ML}(\mathbf{x}_{ML}, \boldsymbol{\sigma}_2)$ are given in Appendix A.2.

5.3 State-Dependent Formulation of the Outer Loop

The outer loop is formulated using the flight path angle and altitude dynamics derived in (36) and (37), respectively. However, there are two possible ways of formulating the outer loop in SDC form, which are now both discussed.

For the first formulation, the state vector and the control vector for the outer loop are defined as

$$\mathbf{x}_{OL} \triangleq [\gamma \quad \chi \quad h]^T, \quad \mathbf{u}_{OL} \triangleq [a_{Y_B} \quad a_{Z_B}]^T.$$

The bias terms contained in (36) are handled by multiplying and dividing these terms by the state h, which never goes to zero. Constructing the required SDC parameterization is then very straightforward, giving

$$\mathbf{A}_{OL}(\mathbf{x}_{OL}) = \begin{bmatrix} 0 & 0 & a_{13} \\ 0 & 0 & a_{23} \\ a_{31} & 0 & 0 \end{bmatrix}, \quad \mathbf{B}_{OL} = \begin{bmatrix} b_{11} & b_{12} \\ b_{21} & b_{22} \\ 0 & 0 \end{bmatrix}, \quad (44)$$

with the resultant coefficients defined in Appendix A.3.

The second alternative formulation follows Cloutier & Stansbery (2002a), using angle of attack and bank angle commands, while issuing a zero sideslip command for a BTT autopilot. However, the controls α and μ appear nonlinearly in (36) as products of sines and cosines. Therefore, in order to bring the dynamics into control-affine form (38), integral control must be applied. Defining the state and control vectors $\mathbf{x}_{OL} \triangleq [\gamma \quad \chi \quad h \quad \alpha \quad \mu]^T$ and $\mathbf{u}_{OL} \triangleq [\dot{\alpha} \quad \dot{\mu}]^T$, bias terms contained in (36) can be handled by multiplying and dividing these terms by the state h. The SDC parameterization can then be constructed in a similar manner as before. Although this alternative formulation increases the order of the state vector by two, it can provide the desired set of controls for BTT missiles using flight path angle commands from the guidance system (Cloutier & Stansbery, 2002a). The former formulation, however, has the advantage of providing acceleration commands to the intermediate loop, which are directly available from sensor measurements, as opposed to estimates of incidence angles required for the second formulation. Therefore, the former formulation proposed here is used with the three-loop topology, whereas, for BTT missiles, use of the inner two-loop structure is proposed.

6. CONTROLLER DESIGN

6.1 Control Design Approaches

For control design of the proposed three-loop structure presented in Fig. 5, any *extended linearization control method* (Çimen, 2010) such as pole placement can be applied. However, recent attention has been directed towards satisfying performance and stability robustness requirements by designing autopilots using *optimal control theory*, because these requirements for current and future missiles necessitate the use of optimally designed multivariable digital flight control systems (Wise, 2007). LQR state feedback designs generally give good performance characteristics and stability margins, with the availability of the states required for implementation. Command tracking is achieved through this framework by augmenting the system with an integrator, and designing the controller for the augmented system. In many practical designs not all the states are available for feedback and, for these problems, H_2 and H_∞ frameworks can be applied. All these methods lead to the various State-Dependent Riccati Equation (SDRE) control methodologies proposed in the literature, such as the SDRE nonlinear regulator, SDRE integral servomechanism, SDRE nonlinear H_2 control, and SDRE nonlinear H_∞ control, which are all viable approaches for controller design. These methods use either *state feedback* or *output feedback* architectures, and are all the product of optimal control based designs.

Using *SDRE nonlinear regulation* with *integral control*, the SDRE controller can be implemented as an *integral servomechanism* to provide a type 1 controller for all three loops in order to perform perfect *tracking* of the loop commands (Çimen, 2010). This is accomplished by first decomposing the state vector $\mathbf{x}$ (which must be available for feedback) as $\mathbf{x}^T = [\mathbf{x}_R{}^T \quad \mathbf{x}_N{}^T]$, where it is desired for the vector components of $\mathbf{x}_R$ (the tracked states) to track a reference, input or command signal $\mathbf{r} \in \mathbb{R}^p$, and $\mathbf{x}_N$ consists

of the nontracked states. The state vector $\mathbf{x}$ is then augmented with $\mathbf{x}_I$, the integral states of $\mathbf{x}_R$. The augmented system becomes

$$\dot{\tilde{\mathbf{x}}} = \tilde{\mathbf{A}}(\tilde{\mathbf{x}}, \boldsymbol{\sigma})\tilde{\mathbf{x}} + \tilde{\mathbf{B}}(\tilde{\mathbf{x}})\mathbf{u},$$

$$\tilde{\mathbf{x}} \triangleq [\mathbf{x}_I^T \quad \mathbf{x}_R^T \quad \mathbf{x}_N^T]^T, \quad \tilde{\mathbf{A}}(\tilde{\mathbf{x}}, \boldsymbol{\sigma}) = \left[\begin{array}{c|c|c} \mathbf{0} & \mathbf{I} & \mathbf{0} \\ \hline \mathbf{0} & \multicolumn{2}{c}{\mathbf{A}(\mathbf{x}, \boldsymbol{\sigma})} \end{array}\right], \quad \tilde{\mathbf{B}}(\tilde{\mathbf{x}}) = \left[\begin{array}{c} \mathbf{0} \\ \hline \mathbf{B}(\mathbf{x}) \end{array}\right]$$

with $\mathbf{A}(\mathbf{x}, \boldsymbol{\sigma})$ and $\mathbf{B}(\mathbf{x})$ derived in Section 5 for each of the three loops. The problem is then formulated as a *nonlinear optimal control problem*, with the minimization of

$$J = \tfrac{1}{2}\int_0^\infty \left\{\tilde{\mathbf{x}}^T\tilde{\mathbf{Q}}(\tilde{\mathbf{x}})\tilde{\mathbf{x}} + \mathbf{u}^T\tilde{\mathbf{R}}(\tilde{\mathbf{x}})\mathbf{u}\right\} dt.$$

Then, by mimicking the LQR formulation, the full-state feedback, robust SDRE integral servo controller becomes

$$\mathbf{u}(\mathbf{x}) = -\tilde{\mathbf{R}}^{-1}(\tilde{\mathbf{x}})\tilde{\mathbf{B}}^T(\tilde{\mathbf{x}})\tilde{\mathbf{P}}(\tilde{\mathbf{x}})\begin{bmatrix} \mathbf{x}_I - \int \mathbf{r}\, dt \\ \mathbf{x}_R - \mathbf{r} \\ \mathbf{x}_N \end{bmatrix},$$

where $\tilde{\mathbf{P}}(\mathbf{x})$ is the unique, symmetric, positive-definite (pointwise stabilizing) solution of the *SDRE*

$$\tilde{\mathbf{P}}(\tilde{\mathbf{x}})\tilde{\mathbf{A}}(\tilde{\mathbf{x}}, \boldsymbol{\sigma}) + \tilde{\mathbf{A}}^T(\tilde{\mathbf{x}}, \boldsymbol{\sigma})\tilde{\mathbf{P}}(\tilde{\mathbf{x}}) - \tilde{\mathbf{P}}(\tilde{\mathbf{x}})\tilde{\mathbf{B}}(\tilde{\mathbf{x}})\tilde{\mathbf{R}}^{-1}(\tilde{\mathbf{x}})\tilde{\mathbf{B}}^T(\tilde{\mathbf{x}})\tilde{\mathbf{P}}(\tilde{\mathbf{x}}) + \tilde{\mathbf{Q}}(\tilde{\mathbf{x}}) = \mathbf{0}.$$

In the absence of the integral states $\mathbf{x}_I$, the above formulation reduces to the SDRE *servomechanism* problem.

6.2 Selection of Design Parameters

The respective vector design parameters $\boldsymbol{\sigma}_1$ and $\boldsymbol{\sigma}_2$ defining the hypersurface of SDC parameterizations given in (40) and (43) (see Appendix A) must now be selected for controller design. A systematic and an effective procedure has been described in Çimen (2010) for selecting the "best" SDC parameterization, which is to attempt to maximize the pointwise controllable spaces of the possible factorizations by computing the state-dependent controllability matrix

$$\mathbf{M}_C(\mathbf{x}, \boldsymbol{\sigma}_i) = [\mathbf{B}(\mathbf{x}) \mid \mathbf{A}(\mathbf{x}, \boldsymbol{\sigma}_i)\mathbf{B}(\mathbf{x}) \mid \cdots \mid \mathbf{A}^{n-1}(\mathbf{x}, \boldsymbol{\sigma}_i)\mathbf{B}(\mathbf{x})], \quad i = 1, 2$$

and evaluate it for different values of $\boldsymbol{\sigma}_1$ and $\boldsymbol{\sigma}_2$. This is clearly the logical choice, since pointwise control effort can be directly linked to these issues (for a detailed discussion with examples, readers may refer to Çimen, 2010).

In order for the SDRE to have a solution, the pointwise detectability condition must also be satisfied (Çimen, 2010). The state-dependent weighting matrix $\tilde{\mathbf{Q}}(\tilde{\mathbf{x}})$ must be selected and tuned for the entire range of flight conditions, in order to maintain good autopilot response over the entire flight envelope (Cloutier & Stansbery, 2001). The state weightings on the tracked outputs, therefore, must be varied at low, medium and high speeds and altitudes until similar performance is achieved for all cases. The state weightings can then be curve fit to a quadratic function of dynamic pressure $\bar{q}$, which is a function of both altitude and airspeed, and hence Mach number (one of the states in the outer loop). Alternatively, they can be calculated online by interpolation.

6.3 Design Genericity

Skid-to-turn (STT) and bank-to-turn (BTT) are the two basic modes of controlling a missile. In the STT mode, the roll angle is either held constant or uncontrolled. This has the major advantage of decoupling roll dynamics from the pitch and yaw dynamics, and delivering faster response than the BTT mode. A BTT missile, on the other hand, allows only positive angles of attack while maintaining small sideslip angles to prevent missile maneuvers from shading the inlet of air-breathing engines in order to increase fuel efficiency and thereby maximize range. The desired orientation is achieved by rolling (banking) the missile so that the plane of maximum aerodynamic normal force is in the desired direction, and the magnitude of the force is controlled by adjusting the angle of attack in that plane.

Recall that maximizing overall missile performance requires choosing the appropriate autopilot command structure for each mission phase. The genericity of the design presented in Sections 4 and 5 thus becomes apparent, where the reference command can be selected as any of the state variables, depending on the specific control mode, intercept scenario, or mission phase. For example, for STT missiles, the tracking command is usually given by $\mathbf{r} = [a_{Y_B}^{com} \quad a_{Z_B}^{com} \quad \mu^{com}]^T$, so that $\mathbf{x}_R$ is defined as $\mathbf{x}_R = [a_{Y_B} \quad a_{Z_B} \quad \mu]^T$, with $\mu^{com} = 0$ such that the bank angle is regulated to zero. For BTT missiles, on the other hand, the autopilot can easily be transformed to follow roll angle and angle-of-attack commands generated by the guidance system (or the outer loop, if desired), so that $\mathbf{r} = [\alpha_{com} \quad \beta_{com} \quad \mu_{com}]^T$ and thus $\mathbf{x}_R = [\alpha \quad \beta \quad \mu]^T$ with $\beta_{com} = 0$, since the sideslip angle must be kept as small as possible during flight. In case of altitude-hold autopilots, the altitude in the outer loop may be selected as the commanded input, so that $r = h^{com}$ and $x_R = h$. The required autopilot command structure then becomes a consequence of the chosen reference commands. If *body rates* are the guidance commands, then only the single inner-loop layer in Fig. 5 is required for autopilot design. Alternatively, for *acceleration* or *incidence angle* commands, the required autopilot topology is given by the inner two-loop structure of Fig. 5. On the other hand, if the guidance algorithm supplies *flight path angle* or *altitude* commands, the complete three-loop autopilot design topology of Fig. 5 is then required. Additionally, several possible combinations can be used for each mission phase by switching between the required command structures within the proposed topology during different phases of flight.

6.4 Performance and Robustness Results

The genericity, performance and robustness of the autopilot design approach developed in the paper has been tested and evaluated on several alternative missile configurations, using different intercept scenarios, and for entire engagements, from launch to intercept, using detailed 6-DOF simulations and Monte Carlo runs. In particular, the developed approach has been used in autopilot design for several hypothetical missile configurations, including a highly unstable missile airframe with canard controls, stable and unstable nonminimum-phase tail-controlled configurations, and a configuration which has combined characteristics, with a separable booster mechanism that switches between thrust vectoring during launch and canard control after separation. In the latter case, different autopilots for vertical launch, midcourse and terminal phases have been successfully implemented for entire engagements, based on different sets of autopilot command structures in Fig. 5. The nonlinear autopilot has been implemented into the simulation and integrated with a high-order control actuation system, as opposed to the second-order dynamics assumed in the autopilot model. Guidance and navigation algorithms were supplied using a strapdown IMU sensor, taking into account sensor location. Simulations were then performed with the nonlinear autopilot solved online at a rate of 1 kHz. Due to space limitations, however, the various sets of simulation results could not be included in the paper, and will be presented during Congress presentation. At this point, however, it is worth mentioning that the inner-, intermediate- and outer-loop SDRE controllers all provide excellent

tracking performance over the full range of flight conditions and throughout the entire operating envelope, for various missile configurations and intercept scenarios. This should not come as a surprise, since outstanding performance of SDRE-based designs for nonlinear missile autopilots have already been demonstrated in several works in the literature (see, for example, Mracek & Cloutier, 1996, 1997; Cloutier & Stansbery, 2001, 2002a; and Vaddi, Menon & Ohlmeyer, 2009). Simulations have shown that at different flight conditions within the flight envelope the time-scaled nonlinear autopilot structure presented in Fig. 5 consistently delivers uniform performance when designed with SDRE control. Thus, the SDRE autopilot provides the same level of performance at all Mach numbers and altitudes. Additionally, since no gain scheduling is required to implement the autopilot, tremendous savings in the design effort can be realized. Moreover, robust performance of the nonlinear autopilot design approach using the SDRE method has been evaluated and validated in the presence of high uncertainties in the aerodynamic coefficients, measurement inaccuracies, noise and delays, INS errors, as well as continuous wind and turbulent atmospheric effects, achieving outstanding performance in all these cases.

7. CONCLUSIONS

In this study, a generic approach to missile autopilot design has been developed using state-dependent nonlinear control. The proposed topology has a three-loop structure. The outer loop uses either flight path angle commands or altitude commands from the guidance law to generate roll angle command together with either body acceleration commands or incidence angle commands, depending on whether the missile flies STT or BTT. The intermediate loop tracks the outer-loop commands by generating commanded body (roll, pitch and yaw) rates. The inner loop then tracks the intermediate loop body rate commands using the control surface deflections. In this topology, any extended linearization control method, such as various SDRE methods, can be applied in the design of all three loops. Full nonlinear and coupled 6-DOF equations of motion describing missile dynamics are derived and used directly in all three loops, where state-dependent nonlinear control is applied in each loop without making any simplifications to the equations. A general form of the hypersurface of SDC parameterizations is constructed for the inner, intermediate and outer loops to carry out the control design. This topology also preserves the inherent time-scale separation between translational and rotational dynamics of the short-period mode, and produces an effective approach to missile autopilot design. Detailed 6-DOF simulations have also indicated that the proposed approach significantly improves gain-scheduled linear autopilots. The generic approach developed in this study for autopilot design can be easily extended to even more general cases, such as advanced missile control problems with thrust vectoring and reaction jets, and even other flight control design problems using the general form of the 6-DOF rigid-body equations of motion in the design of state-dependent nonlinear flight control systems.

ACKNOWLEDGEMENTS

The author would like to thank Prof. M. Kemal Özgören (Middle East Technical University, Turkey) and Mr. Bahadır Çor (ROKETSAN Missiles Industries Inc., Turkey) for providing constructive comments and valuable ideas, which helped significantly improve this paper.

REFERENCES

J. H. Blakelock (1991). *Automatic Control of Aircraft and Missiles*, 2nd Ed., Wiley.

T. Çimen (2010). Systematic and effective design of nonlinear feedback controllers via the state-dependent Riccati equation (SDRE) method. *Annual Reviews in Control, 34*, 32–51.

J. R. Cloutier, and D. T. Stansbery (2001). Nonlinear, hybrid bank-to-turn/skid-to-turn autopilot design. In: *Proc. of the AIAA Guidance, Navigation, and Control Conference*, Montreal, Canada.

J. R. Cloutier, and D. T. Stansbery (2002a). Dynamic conversion of flight path angle commands to body attitude commands. In: *Proc. of the American Control Conference*, Anchorage, AK, USA, 221–225.

J. R. Cloutier, and D. T. Stansbery (2002b). The capabilities and art of state-dependent Riccati equation-based design. In: *Proc. of the American Control Conference*, Anchorage, AK, USA, 86–91.

B. Etkin (2005). *Dynamics of Atmospheric Flight*, Dover Books on Engineering.

J. L. Meriam, and L. G. Kraige (1986). *Engineering Mechanics, Volume 2, Dynamics*, Second Edition, John Wiley & Sons, Inc., New York, NY.

C. P. Mracek, and J. R. Cloutier (1996). Missile longitudinal autopilot design using the state-dependent Riccati equation method. In: *Proc. of the International Conference on Nonlinear Problems in Aviation and Aerospace*, Daytona Beach, FL, USA, 387–396.

C. P. Mracek, and J. R. Cloutier (1997). Full envelope missile longitudinal autopilot design using the state-dependent Riccati equation method. In: *Proc. of the AIAA Guidance, Navigation, and Control Conference*, New Orleans, LA, USA, 1697–1705.

J. N. Nielsen (1988). *Missile Aerodynamics*, AIAA.

B. L. Stevens, and F. L. Lewis (2003). *Aircraft Control and Simulation*, 2nd Ed., John Wiley & Sons.

S. S. Vaddi, P. K. Menon, and E. J. Ohlmeyer (2009). Numerical state-dependent Riccati equation approach for missile integrated guidance control. *AIAA Journal of Guidance, Control, and Dynamics, 32*, 699–703.

K. A. Wise (2007). A trade study on missile autopilot design using optimal control theory. In: *Proc. of the AIAA Guidance, Navigation and Control Conference and Exhibit*, Hilton Head, South Carolina, USA.

K. A. Wise, and D. J. Broy (1998). Agile missile dynamics and control. *AIAA Journal of Guidance, Control, and Dynamics, 21*, 441–449.

P. H. Zipfel (2007). *Modeling and Simulation of Aerospace Vehicle Dynamics*, AIAA.

Appendix A. SDC MATRIX COEFFICIENTS

A.1 Inner-Loop SDC Matrix Coefficients

$$a_{11} = L_p + \sigma_{11} L_{pq} q \qquad a_{12} = M_p + M_{\dot{p}} p + \sigma_{13} M_{\dot{p}r} r \qquad a_{13} = N_p + \sigma_{14} N_{pq} q$$
$$a_{21} = (1-\sigma_{11}) L_{pq} p + \sigma_{12} L_{qr} r \qquad a_{22} = M_q \qquad a_{23} = (1-\sigma_{14}) N_{pq} p + \sigma_{15} N_{qr} r$$
$$a_{31} = L_r + (1-\sigma_{12}) L_{qr} q \qquad a_{32} = M_{\dot{r}} r + (1-\sigma_{13}) M_{\dot{p}r} p \qquad a_{33} = N_r + (1-\sigma_{15}) N_{qr} q$$

A.2 Intermediate-Loop SDC Matrix Coefficients

$$a_{11} = X_{a_X} \sigma_{2,1} M \quad a_{12} = X_{a_Y} \sigma_{2,2} M \quad a_{13} = X_{a_Z} \sigma_{2,3} M$$
$$a_{21} = Y_{a_X} \sigma_{2,4} M \quad a_{22} = Y_{a_Y} \sigma_{2,5} M \quad a_{23} = Y_{a_Z} \sigma_{2,6} M$$
$$a_{31} = Z_{a_X} \sigma_{2,7} M \quad a_{32} = Z_{a_Y} \sigma_{2,8} M \quad a_{33} = Z_{a_Z} \sigma_{2,9} M$$
$$a_{14} = X_{a_X}(1-\sigma_{2,1}) a_{X_B} + X_{a_Y}(1-\sigma_{2,2}) a_{Y_B} + X_{a_Z}(1-\sigma_{2,3}) a_{Z_B} + X_{M^2} M$$
$$a_{24} = Y_{a_X}(1-\sigma_{2,4}) a_{X_B} + Y_{a_Y}(1-\sigma_{2,5}) a_{Y_B} + Y_{a_Z}(1-\sigma_{2,6}) a_{Z_B} + Y_{M^2} M$$
$$a_{34} = Z_{a_X}(1-\sigma_{2,7}) a_{X_B} + Z_{a_Y}(1-\sigma_{2,8}) a_{Y_B} + Z_{a_Z}(1-\sigma_{2,9}) a_{Z_B} + Z_{M^2} M$$
$$a_{41} = \tfrac{1}{a}[\tfrac{1}{3}\tfrac{c_\alpha - 1}{\alpha}\tfrac{c_\beta - 1}{\beta}(\sigma_{2,10} + \sigma_{2,11})\alpha\beta + (c_\alpha - 1)\sigma_{2,13} + (c_\beta - 1)\sigma_{2,14} + 1]$$
$$a_{42} = \tfrac{1}{a}\sigma_{2,15}\, s_\beta$$
$$a_{43} = \tfrac{1}{a}[\sigma_{2,16}\, s_\alpha + \tfrac{1}{3}(c_\beta - 1)(\alpha_{2,17} + \alpha_{2,18}) s_\alpha]$$
$$a_{45} = \tfrac{1}{a}[\tfrac{1}{3}\tfrac{c_\alpha - 1}{\alpha}(c_\beta - 1)(1-\sigma_{2,10} + \sigma_{2,12}) a_{X_B} + \tfrac{c_\alpha - 1}{\alpha}(1-\sigma_{2,13}) a_{X_B} + (1-\sigma_{2,16}) a_{Z_B}\tfrac{s_\alpha}{\alpha} + \tfrac{1}{3}(c_\beta - 1)(2-\alpha_{2,18} - \alpha_{2,19}) a_{Z_B}\tfrac{s_\alpha}{\alpha}]$$
$$a_{46} = \tfrac{1}{a}[\tfrac{1}{3}(c_\alpha - 1)\tfrac{c_\beta - 1}{\beta}(2-\sigma_{2,11} - \sigma_{2,12}) a_{X_B} + \tfrac{c_\beta - 1}{\beta}(1-\sigma_{2,14}) a_{X_B} + (1-\sigma_{2,15}) a_{Y_B}\tfrac{s_\beta}{\beta} + \tfrac{1}{3}\tfrac{c_\beta - 1}{\beta}(1-\alpha_{2,17} + \alpha_{2,19}) a_{Z_B} s_\alpha]$$
$$a_{51} = -\tfrac{1}{Mac_\beta}\sigma_{2,21}\, s_\alpha \qquad a_{53} = \tfrac{1}{Mac_\beta}[1 + (c_\alpha - 1)\sigma_{2,20}] \qquad a_{55} = \tfrac{1}{Mac_\beta}[\tfrac{c_\alpha - 1}{\alpha}(1-\sigma_{2,20}) a_{Z_B} - (1-\sigma_{2,21}) a_{X_B}\tfrac{s_\alpha}{\alpha}]$$
$$a_{61} = -\tfrac{1}{Ma}[\tfrac{1}{3}(c_\alpha - 1)(\sigma_{2,22} + \sigma_{2,23}) s_\beta + \sigma_{2,25}\, s_\beta]$$
$$a_{62} = \tfrac{1}{Ma}[(c_\beta - 1)\sigma_{2,26} + 1]$$
$$a_{63} = -\tfrac{1}{3}\tfrac{1}{Ma}(\sigma_{2,27} + \sigma_{2,28}) s_\alpha\, s_\beta$$
$$a_{65} = -\tfrac{1}{3}\tfrac{1}{Ma} s_\beta[\tfrac{c_\alpha - 1}{\alpha}(1-\sigma_{2,22} + \sigma_{2,24}) a_{X_B} + (1-\sigma_{2,27} + \sigma_{2,29}) a_{Z_B}\tfrac{s_\alpha}{\alpha}]$$
$$a_{66} = -\tfrac{1}{Ma}[\tfrac{1}{3}(c_\alpha - 1)(2-\sigma_{2,23} - \sigma_{2,24}) a_{X_B}\tfrac{s_\beta}{\beta} + (1-\sigma_{2,25}) a_{X_B}\tfrac{s_\beta}{\beta} - \tfrac{c_\beta - 1}{\beta}(1-\sigma_{2,26}) a_{Y_B} + \tfrac{1}{3}(2-\sigma_{2,28} - \sigma_{2,29}) a_{Z_B} s_\alpha\tfrac{s_\beta}{\beta}]$$
$$a_{71} = \tfrac{1}{Ma}[\tfrac{1}{3}(\alpha_{2,30} + \alpha_{2,31}) s_\alpha\, t_\beta + \tfrac{1}{3}(\alpha_{2,33} + \alpha_{2,34}) s_\alpha\, t_\gamma\, s_\mu - \sigma_{2,36}\, c_\alpha\, s_\beta\, t_\gamma\, c_\mu]$$
$$a_{72} = \tfrac{1}{Ma} c_\beta\, t_\gamma\, c_\mu, \qquad a_{73} = \tfrac{1}{Ma}[-\tfrac{1}{3}(\alpha_{2,37} + \alpha_{2,38}) s_\alpha\, s_\beta\, t_\gamma\, c_\mu + \sigma_{2,41}\, c_\alpha\, t_\beta + \sigma_{2,42}\, c_\alpha\, t_\gamma\, s_\mu]$$
$$a_{75} = \tfrac{1}{Ma}[\tfrac{1}{3}(1-\alpha_{2,30} + \alpha_{2,32}) a_{X_B}\, t_\beta + \tfrac{1}{3}(1-\alpha_{2,33} + \alpha_{2,35}) a_{X_B}\, t_\gamma\, s_\mu - \tfrac{1}{3}(1-\alpha_{2,37} + \alpha_{2,39}) a_{Z_B}\, s_\beta\, t_\gamma\, c_\mu]\tfrac{s_\alpha}{\alpha}$$
$$a_{76} = \tfrac{1}{Ma}[\tfrac{1}{3}(2-\alpha_{2,31} - \alpha_{2,32}) a_{X_B}\, s_\alpha\tfrac{1}{c_\beta} - (1-\sigma_{2,36}) a_{X_B}\, c_\alpha\, t_\gamma\, c_\mu - \tfrac{1}{3}(2-\alpha_{2,38} - \alpha_{2,39}) a_{Z_B}\, s_\alpha\, t_\gamma\, c_\mu$$
$$+ (1-\sigma_{2,41}) a_{Z_B}\, c_\alpha\tfrac{1}{c_\beta}]\tfrac{s_\beta}{\beta}$$
$$a_{77} = \tfrac{1}{Ma}[\tfrac{1}{3}(2-\alpha_{2,34} - \alpha_{2,35}) a_{X_B}\, s_\alpha + (1-\sigma_{2,42}) a_{Z_B}\, c_\alpha]\, t_\gamma\tfrac{s_\mu}{\mu}$$

A.3 Outer-Loop SDC Matrix Coefficients

$$a_{13} \triangleq \tfrac{1}{Mab}[(s_\alpha\, c_\mu + c_\alpha\, s_\beta\, s_\mu) a_{X_B} + g_1] \qquad b_{11} \triangleq -\tfrac{1}{Ma} c_\beta\, s_\mu \qquad b_{12} \triangleq -\tfrac{1}{Ma}(c_\alpha\, c_\mu - s_\alpha s_\beta\, s_\mu)$$
$$a_{23} \triangleq \tfrac{1}{Mabc_\gamma}[(s_\alpha\, s_\mu - c_\alpha\, s_\beta\, c_\mu) a_{X_B} + g_2] \qquad b_{21} \triangleq \tfrac{1}{Mac_\gamma} c_\beta\, c_\mu \qquad b_{22} \triangleq -\tfrac{1}{Mac_\gamma}(c_\alpha\, s_\mu + s_\alpha\, s_\beta\, c_\mu)$$
$$a_{31} \triangleq Ma\, s_\gamma / \gamma$$